Mechanism of Primary Charge Photogeneration in Polyfluorene Copolymer/Fullerene Blends and Influence of the Donor/Acceptor Lowest Unoccupied Molecular Orbital Level Offset

ARTICLE *in* THE JOURNAL OF PHYSICAL CHEMISTRY C · JANUARY 2013

Impact Factor: 4.77

READS

5

7 AUTHORS, INCLUDING:

Wei Zhang

Lund University

18 PUBLICATIONS **13** CITATIONS

SEE PROFILE

Rong Hu

11 PUBLICATIONS **58** CITATIONS

SEE PROFILE

Jian-Ping Zhang

Renmin University of China

144 PUBLICATIONS **2,036** CITATIONS

SEE PROFILE

THE JOURNAL OF PHYSICAL CHEMISTRY C

Article

pubs.acs.org/JPCC

Mechanism of Primary Charge Photogeneration in Polyfluorene Copolymer/Fullerene Blends and Influence of the Donor/Acceptor Lowest Unoccupied Molecular Orbital Level Offset

Wei Zhang,[†,‡] Yu-Wei Wang,[†] Rong Hu,[†] Li-Min Fu,[†] Xi-Cheng Ai,[†] Jian-Ping Zhang,*[,†,‡] and Jian-Hui Hou*[,§]

[†]Department of Chemistry, Renmin University of China, Beijing 100872, China

[‡]Center for Condensed Matter Science and Technology, Department of Physics, Harbin Institute of Technology, Harbin 150001, China

[§]State Key Laboratory of Polymer Physics and Chemistry, Beijing National Laboratory for Molecular Sciences, Institute of Chemistry, Chinese Academy of Sciences, Beijing 100190, China

Supporting Information

ABSTRACT: Primary charge photogeneration dynamics in the films of polyfluorene copolymer PFDTBT (poly([2,7-(9,9-bis(3,7-dimethyloctyl)fluorene)]-*alt*-[5,5-(4,7-di-2′-thienyl-2,1,3-benzothiadiazole)])) blended with fullerene derivatives, with variation of fullerene/polymer lowest unoccupied molecular orbital level offsets ($-\Delta E_L$) over 110−320 meV, are investigated by using near-infrared transient absorption spectroscopy under low excitation photon fluence. Time-resolved spectra combined with spectroelectrochemical characterization enable us to verify the signature spectra of the S_1 exciton of the polymer, the interfacial charge transfer (ICT) state, and the charge-separated (CS) state, with which the species-associated kinetics are derived via decomposition of the time-resolved data matrices. For a neat film the interchain CT state is generated irrespective of the excitation photon energy; however, the CS state forms merely upon the above-gap excitation with a quantum yield of 15%, which subsequently recombines into the S_1 exciton within 1 ps. For blend films a dual-path scheme of free charge formation is revealed: The S_1 exciton transforms in a parallel manner into the ICT and CS states with branching ratios Φ_{ICT}:$\Phi_{CS} \approx 3$:1 and time constants of 180−800 fs depending on $-\Delta E_L$. When $-\Delta E_L$ is relatively large, i.e., 0.29 or 0.32 eV for PFDTBT blended with $PC_{61}BOE$ (4-(pentyl-[6,6]-C61)benzene octyl ether) or $PC_{61}BM$ (phenyl-[6,6]-C61-butyric acid methyl ester), respectively, the ICT state further dissociates into the CS state with a time constant of ∼300 ps and an efficiency exceeding 50%. This channel, however, closes when $-\Delta E_L < 0.20$ eV, and the ICT state fully recombines back to the ground state within a few hundred picoseconds. The large ICT-to-CS branching ratio and high dissociation efficiency of the ICT state consolidate the crucial role of this state in photocurrent generation. On the other hand, the process of exciton-to-CS transition is found to obey Marcus's nonadiabatic electron transfer mechanism with a coupling strength $V = 55 \pm 7$ cm^{-1} and a reorganization energy $\lambda = 0.33 \pm 0.02$ eV, whereas the dissociation of the ICT state can be accounted for by Braun−Onsager's model of e^-−h^+ dissociation. The dynamic properties of the ICT state and roles of $-\Delta E_L$ in yielding charge species (ICT and CS) revealed in the present work may shed light on the development of new photovoltaic materials.

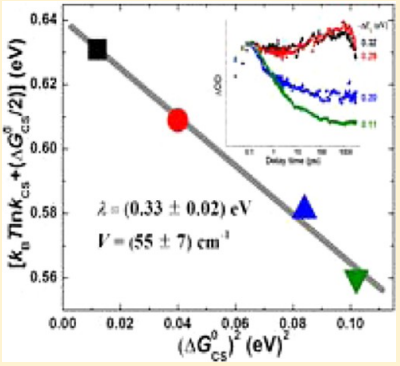

1. INTRODUCTION

Organic solar cells based on the bulk heterojunction (BHJ) by mixing conjugated polymers with fullerene derivatives have achieved a power conversion efficiency (PCE) exceeding 8%.[1−3] New molecular designs of the hole-conducting polymers[4−10] and electron-conducting fullerenes,[11−14] morphological optimization of the photoactive layers,[15−19] and configurational improvement of the devices[1,2,20−22] have been shown to be effective for the PCE enhancement. On the other hand, the dynamics of light harvesting and charge photogeneration/recombination have been investigated extensively for the BHJ layers as well as for the integrated devices, since understanding the elementary processes of light conversion, in connection with the morphologies and molecular structures of photovoltaic materials and with the operating conditions as well, is beneficial for attaining the theoretical limit of PCE for the single-layer devices (11%).[23,24]

Regarding charge photogeneration, the primary electronic excitation of a polymer via light absorption is often referred to as the Frenkel-type exciton, a pair consisting of a tightly bound electron (e^-) and hole (h^+) that migrate in the polymer phase or dissociate at the polymer/fullerene interface to yield free

Received: August 25, 2012
Revised: November 14, 2012
Published: December 3, 2012

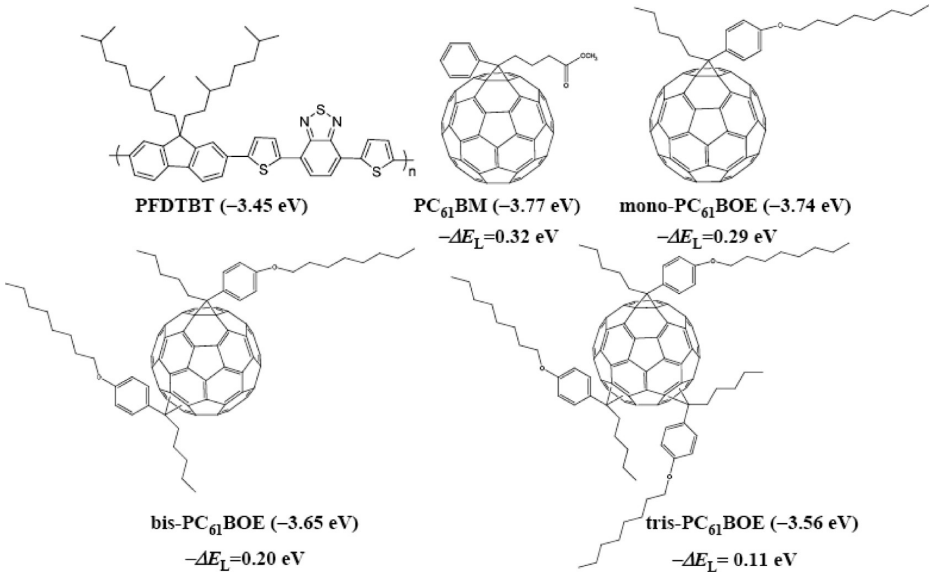

Figure 1. Molecular structures of PFDTBT and fullerene derivatives $PC_{61}BM$, mono-$PC_{61}BOE$, bis-$PC_{61}BOE$, and tris-$PC_{61}BOE$. The electrochemical LUMO energies are given in parentheses with error bars below ±0.01, and the fullerene/polymer LUMO level offsets are indicated ($-\Delta E_L$).

charge carriers.[25] Due to the weak dielectric screening inherent to organic photovoltaic materials of low relative dielectric constants (ε_r = 2−4),[26−28] the electrostatic binding energy of an exciton (0.5−1 eV) is substantially larger than the thermal energy k_BT (0.026 eV, k_B = Boltzmann's constant, T = 300 K).[29,30] It is generally believed that, for efficient charge carrier generation, a sum of free energy is needed for the exciton dissociation.[24,30,31] However, there exist alternative views based on ultrafast spectroscopic studies on the neat film of PCDTBT (poly[*N*-9″-heptadecanyl-2,7-carbazole-*alt*-5,5-(4′,7′-di-2-thienyl-2′,1′,3′-benzothiadiazole)]) and its blends with $PC_{71}BM$ (phenyl-[6,6]-C71-butyric acid methyl ester): Charges can be the primary events of photoexcitation prior to the exciton formation, and hence, the exciton dissociation is irrelevant to the charge transfer reactions.[32,33]

The size of free energy spent on exciton dissociation is evidently an important issue, because it is critically relevant to the usable energy of output electrons and hence to the PCE. In this context, the free energy for promoting the PPV (poly[2-methoxy-5-((2′-ethylhexyl)oxy)-*p*-phenylenevinylene]) intrachain exciton to the PPV/CN-PPV (poly[2,5,2′,5′-(tetrahexyloxy)-7,8′-dicyano-di-*p*-phenylenevinylene]) interchain charge transfer (CT) state was suggested to be ∼0.35 eV.[34] However, the validity of this value to other types of polymer/polymer or polymer/fullerene blends needs to be further proved.[23,35] For instance, despite the small fullerene/polymer lowest unoccupied molecular orbital (LUMO) level offset, $-\Delta E_L \approx 0.1$ eV, the solar cell based on PCPDTBT poly[2,6-(4,4-bis-(2-ethylhexyl)-4*H*-cyclopenta[2,1-b;3,4-b′]-dithiophene)-*alt*-4,7-(2,1,3-benzothiadiazole)] and $PC_{71}BM$ shows a PCE as high as 5%.[10] In addition, efficient charge photogeneration was also found for other organic photovoltaic materials with relatively small $-\Delta E_L$, for which the interaction between electronic and nuclear coordinates was suggested to play an important role.[36] In a series of studies with systematic tuning of the LUMO levels of polymers[27,37−39] and those of fullerene or non-fullerene electron acceptors,[40] the $-\Delta E_L$ was shown to correlate positively with the yield of polymer cationic polarons measured at 1 μs after the light flash. In these studies, however, the $-\Delta E_L$ values were mostly above 0.5 eV and the polaron photogeneration was not examined on ultrafast time scales, in effect hampering the assessment of the requisite $-\Delta E_L$ for driving the interfacial charge separation.

Exciton dissociation involves the polymer/fullerene interfacial charge transfer (ICT) state, corresponding to the geminate pair or polaron pair frequently discussed in the literature.[30,47−50] The ICT states may be categorized into energetically relaxed and unrelaxed (hot) states. The former recombines irreversibly into the ground state and thus acts as a trap of excitations and charges.[32,41,42] This state can be unambiguously probed by photo- or electroluminescence or by direct photoabsorption from the ground state for a range of polymer/polymer and polymer/fullerene combinations.[30,31,43−46] The hot ICT state possessing excess energy is potent to dissociate into the fully charge-separated (CS) state that is detected as the polymer radical cation ($P^{\bullet+}$) by transient absorption (TA) spectroscopy. Note that the terms "relaxed ICT state" and "hot ICT state" underline their energetic and dynamics properties, respectively, both of which play crucial roles in efficient light conversion. For instance, the energy level of the relaxed CT state is relevant to the open-circuit voltage (V_{OC}),[31,41] whereas the ICT state, a potent precursor of the CS state, highly influences the photocurrent.[42,47,48,50] In this study, the excitation and charge dynamics are examined on ultrafast time scales, implicitly meaning that the ICT states are unrelaxed states. In addition, the CS state will be used as a synonym for the polaron $P^{\bullet+}$, and both the ICT and the CS states are regarded as charge species in the sense that they have experienced a large extent of or complete charge transfer across the polymer/fullerene interfaces.

Concerning the charge photogeneration mechanisms of the photovoltaic materials based on donor (D)/acceptor (A) alternating copolymers, a sequential model of charge photogeneration, exciton → ICT → CS, has been proposed for APFO3 (poly[2,7-(9,9-dioctylfluorene)-*alt*-5,5-(4,7′-di-2-thienyl-2′,1′,3- benzothiadiazole)]) blended with fullerenes.[47,48,51] However, for the close analogue poly(2,7-carbazole) copolymer PCDTBT, the exciton was suggested to dissociate in a parallel

dx.doi.org/10.1021/jp308442t | J. Phys. Chem. C 2013, 117, 735−749

manner into the ICT and CS states in the PCDTBT/$PC_{70}BM$ blends, while the possible interconversion between them remained unclear.[32] Further investigation on the PCDTBT/$PC_{61}BM$ blends confirmed the parallel paths of free charge formation, elucidated the ICT-to-CS branching ratio (1:9), and concluded that the ICT state is not a precursor of the CS state.[52] Thus, the ICT state for PCDTBT/PCBM may act as an unwanted trap state that recombines back to the ground state, whereas that for APFO3/PCBM may mediate the free charge formation.

To justify the possible roles of the ICT state in charge photogeneration, it is crucial to evaluate the ICT-to-CS branching ratio and dissociation/recombination competition of the ICT state. Such information acquired by means of ultrafast time-resolved spectroscopies is often complicated by the spectral and temporal superposition of the neutral and charge species. Particularly, the absorption spectra of the ICT states are generally thought to be indistinguishable from those of the CS states,[23,53−55] although the ICT states of numerous π-conjugated polymers were previously detected by photoinduced absorption (PA) spectroscopy in the near- to middle-infrared spectral regions.[47,56] To evaluate the ICT-to-CS partition and to differentiate the species-associated temporal evolution profiles, it is necessary to obtain the signature spectra of the individual transient species involved in the ultrafast spectral dynamics. However, direct verification of the ICT state by ultrafast TA spectroscopy has not been realized to date, and consequently, the information on the ultrafast dynamics of this state has relied on the model analyses of ultrafast kinetics at a limited number of probing wavelengths.[48,52]

The present work is intended to elucidate the charge photogeneration mechanisms with an emphasis on the possible roles of the ICT state. The targeting materials include the high-performance polyfluorene copolymer PFDTBT (poly([2,7-(9,9-bis(3,7-dimethyloctyl)fluorene)]-*alt*-[5,5-(4,7-di-2′-thienyl-2,1,3-benzothiadiazole)]))[57,58] and a few newly synthesized fullerenes (Figure 1). $-\Delta E_L$ is tuned systematically from 110 to 320 meV by varying the substituent to the fullerenes, so as to examine the influence of $-\Delta E_L$ on the interfacial charge transfer reactions initiated from the polymer exciton, as well as on the processes of ICT state dissociation. To this end, we have carried out ultrafast TA measurements in the near-infrared region (850−1350 nm) for the neat PFDTBT and blend PFDTBT/fullerene films. The time-resolved spectra combined with the spectroelectrochemical data allow the signature spectra and species-associated evolution kinetics to be derived without invoking any analytical models. The crucial roles of polymer/fullerene interfaces are underlined by comparing the primary exciton and charge photogeneration dynamics of the neat film to those of the blend films. The results have established the parallel mechanism of charge photogeneration in the PFDTBT/fullerene blends, redressing the sequential mechanism previously proposed in ref 48. The ICT state is found to act as either a trap or a precursor of free charges depending on the magnitude of $-\Delta E_L$. The results are discussed in terms of Marcus's theory of nonadiabetic electron transfer reactions[59] and Braun−Onsager's model of e^-−h^+ pair dissociation in disordered solids.[60,61]

2. MATERIALS AND METHODS

2.1. Polymer and Fullerene Derivative syntheses and Film Preparation. The PFDTBT copolymer was synthesized following reported methods.[57,58] The molecular weight was M_n = 20 K, and the PDI was 1.3. $PC_{61}BM$ (~99%) was used as received from Aldrich. Other fullerene derivatives, mono-$PC_{61}BOE$ (4-(pentyl-[6,6]-C61)benzene octyl ether), bis-$PC_{61}BOE$ (4-(pentyl-[6,6]-C61)benzene octyl ether bisadducts), and tris-$PC_{61}BOE$ (4-(pentyl-[6,6]-C61)benzene octyl ether trisadducts), were synthesized following the tosylhydrazone route.[62] Figure 1 shows the molecular structures of PFDTBT and the fullerene derivatives. In film preparation, neat PFDTBT or its blends with the fullerene derivatives (1:3, w/w, a ratio for device fabrication[58]) were dissolved in *o*-dichlorobenzene (*o*-DCB) to obtain the 12.5 mg mL^{-1} solutions. Quartz substrates were treated by ultrasonication in detergent and washed successively with deionized water, acetone, ethanol, and isopropyl alcohol, and the films were spin-coated (neat, 600 rpm, 40 s; blends, 800 rpm, 30 s) onto them. The preparation was carried out in a glovebox under an argon atmosphere (oxygen concentration <0.1 ppm). The film thickness, typically ~90 nm, was determined with an Alpha-Skep surface profiler (KLA-Tencor).

2.2. Steady-State Spectroscopy. UV−vis absorption spectra were recorded on a Cary-50 (Varian) absorption spectrometer. Spectroelectrochemical measurements for the neat or the blend films were carried out with a trielectrode configuration consisting of a working electrode (PFDTBT film on ITO glass), a counter electrode (platinum wire), and a reference electrode (Ag^+/Ag, $AgNO_3$ (0.01 M) and hexafluorophosphate (0.1 M) in acetonitrile), which were assembled in a quartz cell having an effective optical path length of 2 mm. The electrolyte solution was hexafluorophosphate (0.1 M) in acetonitrile. The electrical potential applied across the reference and working electrodes was 0.5 V. The spectroelectrochemical cell was mounted on a spectrometer having a spectral response range of 200−2200 nm (Hitachi, U-4100).

2.3. Electrochemistry. The cyclic voltammograms of mono-$PC_{61}BOE$, bis-$PC_{61}BOE$, tris-$PC_{61}BOE$, and $PC_{61}BM$ dissolved in a binary solvent of *o*-DCB and acetonitrile (5:1, v/v) with 0.1 M $TBAPF_6$ (tetrabutylammonium hexafluorophosphate) were recorded on an electrochemical workstation (CHI650D), for which a glassy carbon working electrode (diameter, 2 mm), a platinum counter electrode, and a Ag/Ag^+ reference electrode (0.01 M $AgNO_3$ in acetonitrile) were used. PFDTBT was prepared as a thin film on the working electrode instead of being dissolved in solution, and pure acetonitrile rather than the binary solvent was used in the voltammetric measurement. All of the measurements were corrected against the ferrocene/ferrocenium couple (Fc/Fc^+) as an internal standard, and the LUMO energies thus determined are indicated in Figure 1. (For more details see the Supporting Information, section S1) The LUMO energy of $PC_{61}BM$, −3.77 eV, falls into the range of documented values between −3.7 and −4.3 eV.[31] The LUMO and HOMO levels of PFDTBT are −3.45 and −5.55 eV, respectively. The latter agrees well with the literature values varying from −5.5 eV[58] to −5.55 eV,[41] whereas the former deviates from the reported value, −3.6 eV, as estimated by adding the optical band gap (E_g =1.9 eV) to the HOMO energy or obtained from the cyclic voltammetry of the *o*-DCB solution of PFDTBT.[41] We adopt the LUMO level determined in the present work, as it was for the PFDTBT film, closer to the reality of the subsequent spectroscopic studies.

2.4. Near-Infrared Ultrafast TA Spectroscopy. The apparatus is briefly described below. An optical parametric amplifier (OPA-800 CF-1, Spectra Physics) pumped by a regenerative amplifier (SPTF-100F-1KHPR, Spectra Physics)

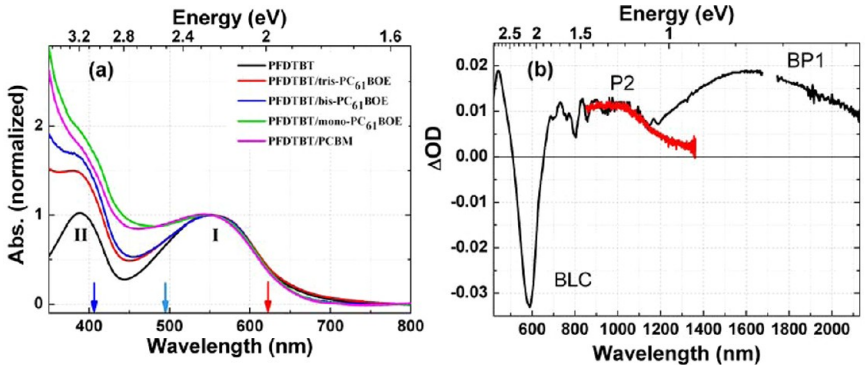

Figure 2. (a) Normalized UV–vis absorption spectra of PFDTBT neat and PFDTBT/fullerene blend films (1:3, w/w). Arrows point to the excitation wavelengths used in the ultrafast TA measurements (λ_{ex} = 413, 490, and 620 nm). (b) Spectroelectrochemical absorption spectrum of the neat PFDTBT film (black) and arbitrarily scaled TA spectrum (red) of the PFDTBT/PC_{61}BM blend (1:3, w/w) recorded at Δt = 2 ns under λ_{ex} = 413 nm.

provided the actinic laser pulses at the desired wavelengths (~120 fs, full width at half-maximum). The continuum probe (800–1400 nm) generated from a 3 mm thick sapphire plate was detected after interrogation of the excited volume of sample by an InGaAs detector (OMA-V, Princeton Instruments) attached to an imaging spectrograph (SpectraPro 2300i). To ensure that each laser shot would excite the sample fully relaxed from the previous excitation, the laser system was run at a repetition rate of 333 Hz. To prevent the films from photodegradation, the films sandwiched with quartz slices were kept in a vacuum. A mechanical chopper (model 75158, Newport) was set in the pump beam to regulate the pump "on" and "off" for a pair of sequential actinic pulses. The magic-angle scheme was used on the pump–probe measurement. To improve the signal-to-noise ratio, each transient spectrum was obtained by averaging 500 individual measurements, and the typical detection sensitivity of the difference absorption (ΔOD) was better than 10^{-4}. The cross correlation trace between the pump and the probe pulses was taken as the instrumental response function (IRF), and the temporal resolution was 160 fs as the full width at half-maximum (fwhm) of the IRF. The time-resolved absorption spectra were corrected against group velocity dispersion. All measurements were carried out at room temperature (296 K).

3. RESULTS

3.1. Spectroscopic Characterization of Radical Cationic PFDTBT. On the basis of a recent quantum chemical study on the polyfluorene copolymer DiO-PFDTBT comprising the alternating 9,9-dioctyl-9*H*-fluorene and 4,7-dithiophene-2-ylbenzo[1,2,5]thiadiazole (TBT) units,[51,63] we attribute the major absorption of the neat PFDTBT film at 554 nm (Figure 2a, band I) to the optical transition from the ground state to the intramolecular charge transfer state, shifting the electron density toward the TBT unit ($S_1 \leftarrow S_0$). The shorter wavelength absorption at 389 nm (Figure 2a, band II) is ascribed to the transition to the excitonic state delocalized over the π-conjugated fluorene–thiophene backbone ($S_2 \leftarrow S_0$). These spectral assignments are rationalized by the fact that PFDTBT differs from DiO-PFDTBT only in the alkyl chain (dimethyloctyl vs dioctyl). It is noteworthy that optimization of the size/shape of the side chain can improve the solubility and hence the photovoltaic performance of PFDTBT.[58]

The spectroelectrochemical spectrum of the PFDTBT film in Figure 2b is characterized by a strong absorption peaking at 440 nm, a bleaching of the ground-state absorption at 590 nm (BLC), and a red-to-near-infrared broad absorption consisting of two overlapped sub-bands (P2 and BP1) with an isosbestic point at ~1150 nm. The origin of the absorption band at 440 nm overlapping with the ground-state bleaching is unclear,[64] whereas the assignments of the near-infrared absorption are made below.

3.1.1. Spectroelectrochemical and TA Spectra at 700–1300 nm. In the case of P3HT (poly(3-hexylthiophene)), the polaron $P3HT^{\bullet+}$ exhibits a pair of broad absorption bands: a near-infrared one (650–1150 nm) originating from the SOMO-to-LUMO transition and a middle infrared one (1200–6000 nm) arising from the HOMO-to-SOMO transition, which are denoted P2 and P1, respectively.[65,66] Both P2 and P1 bands of $P3HT^{\bullet+}$ had been detected in the ultrafast TA measurements.[67,68] In the case of PFDTBT, the spectroelectrochemical bands over 700–1150 and 1150–2000 nm, respectively, seem analogous to the P2 and P1 bands of $P3HT^{\bullet+}$. However, the dual-band feature does not appear in the TA spectrum as seen from Figure 2b. This TA spectrum agrees with the absorption spectrum of the polaron $APFO3^{\bullet+}$ reported in the spectral region up to ~950 nm[48] and also resembles the polaron spectra of the PCDTBT analogues with heneicosanyl[52] or heptadecanyl[56] as the alkyl side chain attached to the carbazole comonomer. Particularly, the TA spectrum in Figure 2b agrees with the photoinduced absorption spectrum of $PCDTBT^{\bullet+}$ as a single band at 800–1300 nm with a weak extension to 1.8 μm.[52] On the basis of the literature data and excellent agreement between the TA spectrum and the spectroelectrochemical band P2, we assign the TA spectrum and P2 band in Figure 2b to the characteristic absorption of $PFDTBT^{\bullet+}$ (hereafter $P^{\bullet+}$).

3.1.2. Spectroelectrochemical Spectrum at 1150–2000 nm. Previous electron spin resonance combined with optical spectroscopic studies revealed that, for oligothiophenes (nT) with extrapolation to polythiophenes, the bipolaron (nT^{2+}) absorption band denoted as BP1 locates to the longer wavelength side of the P2 band of the cationic polaron ($nT^{\bullet+}$).[69] We therefore tentatively attribute the 1150–2000 nm band of the electrospectrochemical spectrum in Figure 2b to the bipolaron absorption of $PFDTBT^{2+}$, which is reasonable in viewing the successive electro-oxidation of the neat PFDTBT film. Note that, for the PFDTBT/PC_{61}BM blend subjected to photoexcitation, the bipolaron species $PFDTBT^{2+}$ could not be generated and hence was not present in the TA spectrum.

dx.doi.org/10.1021/jp308442t | J. Phys. Chem. C 2013, 117, 735–749

The TA results below show that, at a delay time (Δt) later than 1 ns, the polaron $P^{\bullet+}$ becomes predominant over other transient species. Therefore, the TA spectrum at Δt = 2 ns in Figure 2b originates solely from $P^{\bullet+}$ absorption. On the basis of the signature spectra of $P^{\bullet+}$ determined by both spectroelectrochemistry and TA measurements, we are able to obtain, via spectral decomposition, the signature absorption spectrum of $P^{\bullet+}$ as shown in Figure S2 (P2, Supporting Information), which is characterized by a broad-band absorption centered at ~950 nm with a red wing extension to 1300 nm. The other broad-band spectrum from the spectral decomposition is attributable to the $PFDTBT^{2+}$ absorption (BP1), which covers 1100−2000 nm with a maximum at ~1650 nm.

3.2. Spectral Dynamics of the Neat and Blend Films and Influences from $-\Delta E_L$ and the Excitation Photon Energy. Figure 3 shows the TA spectra for the neat and blend films following the pulsed photoexcitation at 620 nm corresponding to the red edge of the $S_1 \leftarrow S_0$ absorption. (For more detailed spectral dynamics see the Supporting Information, Figure S3.) At Δt = 0.13 ps when the ΔOD amplitude is highest (Figure 3a), the neat PFDTBT film exhibits a major absorption band over 1050−1350 nm along with a relatively weaker bump at 850−1050 nm. We have confirmed that under similar excitation conditions neat fullerene films show rather weak and almost featureless background TA signals (data not shown); therefore, the 850−1050 nm features do not originate from the excited-state fullerenes. For the blend films, all of the weaker bumps remain unrelaxed, whereas the major absorption decreases in the order of PFDTBT/tris-PC_{61}BOE, PFDTBT/bis-PC_{61}BOE, PFDTBT/mono-PC_{61}BOE, and PFDTBT/PC_{61}BM with $-\Delta E_L$ increasing from 0.11 to 0.32 eV. The absorption over 1050−1350 nm nearly vanishes in the cases of $-\Delta E_L$ > 0.20 eV.

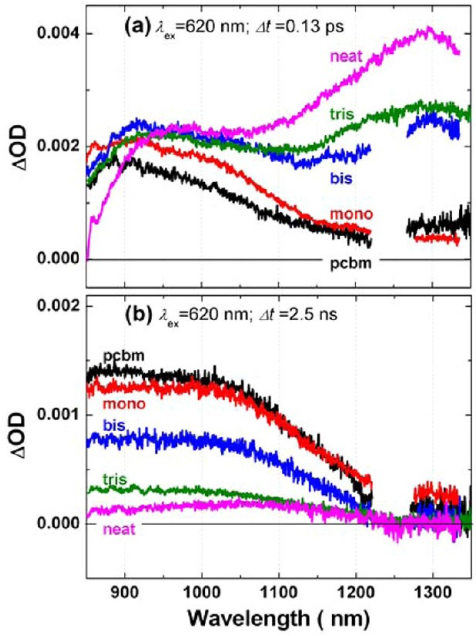

Figure 3. TA spectra at the indicated delay times after photoexcitation at 620 nm. The neat PFDTBT film is denoted "neat", and "tris", "bis", "mono", and "pcbm", respectively, refer to the blend films of PFDTBT mixed with tris-PC_{61}BOE, bis-PC_{61}BOE, mono-PC_{61}BOE, and PC_{61}BM (1:3, w/w). The excitation photon fluence was 9.1 × 10^{12} photons·cm^{-2}·$pulse^{-1}$.

At Δt = 2.5 ns (Figure 3b), the spectral patterns of the blend films are similar to each other; however, the ΔOD amplitudes increase substantially from the neat to the blend films following the aforementioned order. These results demonstrate the intimate correlation of $-\Delta E_L$ to the spectral dynamics of the polymer/fullerene blends.

To examine the effect of the photon energy on the ultrafast excitation/charge dynamics of the neat and blend films, we applied higher photon energy excitation at 413 nm corresponding to the maximum of the $S_2 \leftarrow S_0$ absorption, and the spectral dynamics are illustrated in Figure 4. (For more detailed spectral dynamics see the Supporting Information, Figure S3.) At Δt = 0.13 ps (Figure 4a), the relative ΔOD amplitudes at 1050−1350 nm are apparently lower compared to those in the case of 620 nm photoexcitation, whereas the 850−1250 nm absorption resembles that under 620 nm excitation. We have also examined the spectral dynamics of the neat and blend films photoexcited at 490 nm corresponding to the blue edge of the $S_1 \leftarrow S_0$ absorption, and the red-to-blue relative ΔOD amplitude is between those in the cases of photoexcitation at 620 and 413 nm (Figure S4, Supporting Information). At Δt = 2.5 ns (Figure 4b), the transient spectra under photoexcitation at 413 nm resemble closely those under 620 nm excitation except that the higher photon energy induces a relatively larger ΔOD amplitude at 850−1050 nm. Taking the above results together, we see that both the $-\Delta E_L$ and the excitation photon energy highly influence the spectral dynamics, the implications of which are considered in the Discussion.

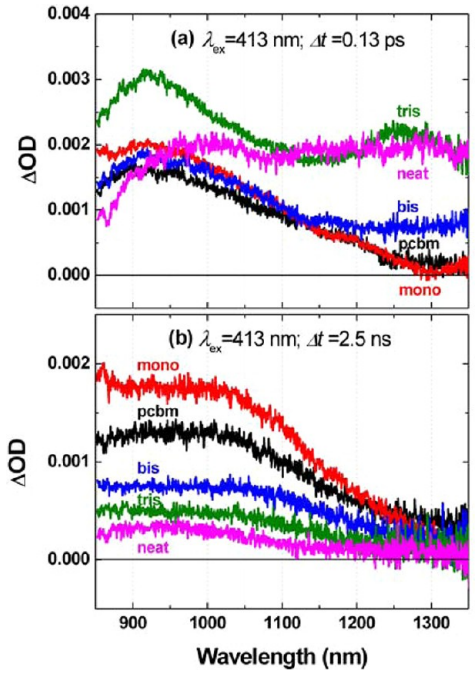

Figure 4. TA spectra at the indicated delay times following the pulsed photoexcitation at 413 nm. The neat PFDTBT film is denoted "neat", and "tris", "bis", "mono", and "pcbm", respectively, refer to the blend films of PFDTBT mixed with tris-PC_{61}BOE, bis-PC_{61}BOE, mono-PC_{61}BOE, and PC_{61}BM (1:3, w/w). The excitation photon fluence was (0.8−3.0) × 10^{13} photons·cm^{-2}·$pulse^{-1}$.

3.3. Signature Spectra of the S_1 Exciton, the ICT State, and $P^{\bullet+}$. The spectral dynamics with an influence from $-\Delta E_L$ and the excitation photon energy provide us with a unique

dx.doi.org/10.1021/jp308442t | J. Phys. Chem. C 2013, 117, 735−749

opportunity to derive the signature spectra of the polymer exciton and ICT and CS states.

3.3.1. Polymer Exciton. The transient spectrum of the neat PFDTBT film in Figure 3a comprises the contribution from the $S_n \leftarrow S_1$ excited-state absorption, because under the band gap photoexcitation, the S_1 exciton as a form of primary excitation is naturally expected. Immediately following the pulsed photoexcitaiton of the neat PFDTBT film (Δt = 0.0 ps), the blue (850−1050 nm) and red (1050−1350 nm) features appeared simultaneously. However, when the delay time elapsed to a few picoseconds, the blue band disappeared, leaving the broad-band absorption alone at 850−1350 nm (Figure S3, Supporting Information). We therefore take an average of the transients in the vicinity of Δt = 100 ps as the signature absorption spectrum of the S_1 exciton (Figure 5a), which does not vary with a change of the excitation wavelength. Note that the blue feature does not show up in the signature spectrum of the S_1 exciton.

3.3.2. CS State ($P^{\bullet+}$). As seen from Figures 3b and 4b, the TA spectra at Δt = 2.5 ns for different blend films are similar to each other irrespective to the excitation wavelengths, and they are all in agreement with the P2 band of the spectroelectrochemical spectrum of $P^{\bullet+}$ (Figure 2b). We therefore adopt the 2.5 ns transient of the PFDTBT/PC_{61}BM film as the signature spectrum of $P^{\bullet+}$ (Figure 5a).

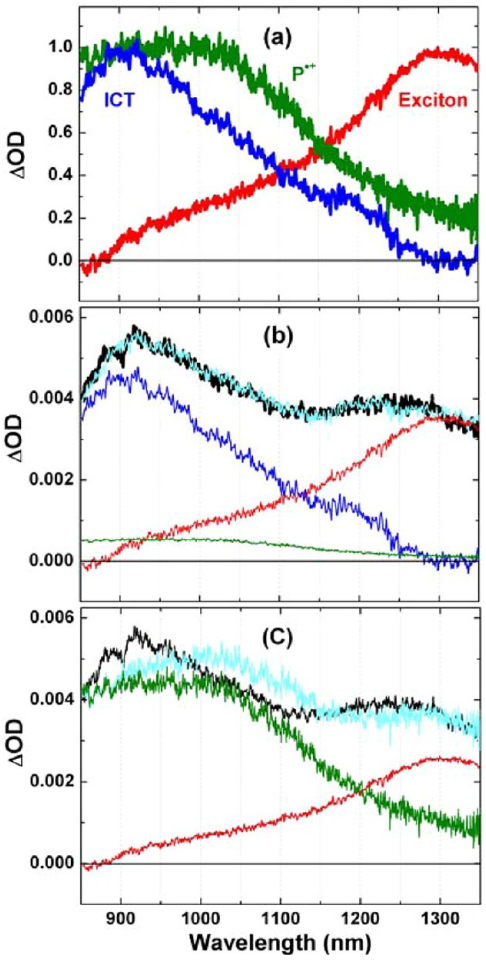

Figure 5. (a) Signature spectra of the S_1 exciton, ICT state, and CS state ($P^{\bullet+}$). (b) Transient spectrum (black) of the PFDTBT/tris-PC_{61}BOE blend (1:3, w/w) at Δt = 0.13 ps along with the least-squares fitting curve (cyanine) calculated from a linear combination of the signature spectra of the S_1 exciton (red), ICT (blue), and $P^{\bullet+}$ (green) (excitation photon fluence 2.3 × 10^{13} photons·cm^{-2}·$pulse^{-1}$, λ_{ex} = 490 nm). (c) Fitting results of the same transient spectrum as in (b) without incorporation of the ICT signature.

3.3.3. ICT State. For the blend films, the TA transients at a delay time of 0.13 ps show the aforementioned blue and red absorption features irrespective of the excitation wavelengths (Figures 3a and 4a). However, with respect to PFDTBT/tris-PC_{61}BOE and PFDTBT/bis-PC_{61}BOE blends having $-\Delta E_L$ below 0.20 eV, the S_1 exciton absorptions are rather weak for PFDTBT/PC_{61}BM and PFDTBT/mono-PC_{61}BOE blends having $-\Delta E_L$ above 0.20 eV, most likely owing to the efficient exciton dissociation. From the 0.13 ps transients of PFDTBT/tris-PC_{61}BOE, we see that, depending on the excitation wavelength, the amplitudes of the 850−1050 nm features are comparable to or even stronger than those of the S_1 exciton absorption (see also Figures S3 and S4, Supporting Information). At Δt = 0.13 ps, a substantial amount of undissociated ICT states are expected for the PFDTBT/tris-PC_{61}BOE blend because of its small $-\Delta E_L$. Similar to the absorption of $P^{\bullet+}$, the absorption of the ICT state at 1300 nm is negligibly small. We then normalized the S_1 exciton spectrum to the 0.13 ps transient of PFDTBT/tris-PC_{61}BOE at 1300 nm and subtracted the former from the latter to obtain the signature spectrum of the ICT state (Figure 5a). The interference of $P^{\bullet+}$ absorption in the resultant ICT spectrum is minimized judging from the 6-fold smaller magnitude of $P^{\bullet+}$ at 2.5 ns than that of ICT at 0.13 ps (Figures 3 and 4). As seen from Figure 5a, the ICT signature spectrum, which is found to be independent of the excitation wavelength, differs distinctly from those of $P^{\bullet+}$ and the S_1 exciton in spectral patterns.

Verification of the signature spectra is exemplified in Figure 5b, showing that a transient spectrum can be satisfactorily simulated by a linear combination of the signature spectra, $\Delta OD(\lambda,\Delta t)$ = $Amp_0(\Delta t)$·exciton(λ) + $Amp_1(\Delta t)$·ICT(λ) + $Amp_2(\Delta t)$·polaron(λ). However, the same spectrum cannot be reassembled without incorporation of the ICT spectrum (Figure 5c). By simulating each set of the time-resolved absorption spectra, we are able to decompose the superimposed absorption spectra of the S_1 exciton and charge species and, concomitantly, to obtain the species-associated kinetics (Amp-(Δt)) of the ICT and CS states.

3.4. Ultrafast Kinetics of Charge Photogeneration in PFDTBT/Fullerene Blend Films. Judging from the signature spectra in Figure 5, the kinetics at λ_{pr} = 1000 nm collectively probe the exciton, the ICT state, and $P^{\bullet+}$. However, those at λ_{pr} = 1300 nm are dominated by the exciton absorption and hence can give rise to the S_1 exciton decay time constants with minimized interference from the charge species. The apparent S_1 exciton lifetime[70] for the neat PFDTBT film derived from the TA kinetics is $\langle\tau\rangle \approx$ 600 ps, which differs from that measured by time-resolved fluorescence spectroscopy, $\langle\tau\rangle \approx$ 380 ps, at probing wavelengths of 720−760 nm (Supporting Information, section S5). The apparent discrepancy is considered to originate from the contribution from different transient species to the TA and fluorescence kinetics. The apparent S_1 exciton lifetime is in good agreement with that determined for the neat PCDTBT film (600 ps).[52] It is worth noting that both TA and fluorescence kinetics decayed nonexponentially: The TA kinetics consisted of the decay components with time constants of 2.3 ps (22%), 46 ps (51%), and 670 ps (27%), while the fluorescence kinetics consisted of the 66 ps (68%) and 475 ps (32%) components. Among them

the picosecond component is attributed to the singlet−singlet excitation annihilation; those of a few tens of to a few hundred picoseconds, respectively, are ascribed to the excitation energy transfer/relaxation in the PFDTBT film and depopulation of the S_1 exciton. The significant excitation transfer/relaxation is due to the considerable energetic disorder of ∼50 meV (Supporting Information, section S5), which is in agreement with the value reported for the neat PCDTBT film (70 meV).[52]

As shown in Figure 6a, the S_1 exciton lifetimes for the blends are prolonged systematically from 0.18 to 0.80 ps with variation

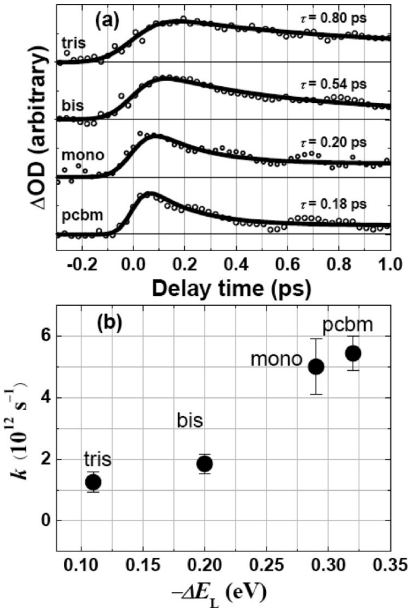

Figure 6. (a) Kinetics of the S_1 exciton probed at 1300 nm for the PFDTBT/tris-PC_{61}BOE (tris), PFDTBT/bis-PC_{61}BOE (bis), PFDTBT/mono-PC_{61}BOE (mono), and PFDTBT/PC_{61}BM (pcbm) blends (1:3, w/w) (excitation photon fluence 9.1 × 10^{12} photons·cm^{-2}·$pulse^{-1}$, λ_{ex} = 620 nm). The indicated exciton lifetimes (τ) were derived from least-squares curve fitting to a biexponential model function with the second lifetime set to infinity. (b) Decay rates of the S_1 exciton ($k = 1/\tau$) plotted against $-\Delta E_L$.

of the fullerene derivatives from PC_{61}BM to tris-PC_{61}BOE, as more clearly illustrated by plotting the decay rate ($k = 1/\tau$) against $-\Delta E_L$ (Figure 6b). Correlation between the exciton lifetime and $-\Delta E_L$ was previously observed for the DiO-PFDTBT/fullerene blends, where the lifetimes shortened from 200 to 100 fs when $-\Delta E_L$ increased from 0.6 eV (PC_{61}BM or PC_{71}BM) to 0.8 eV ([70]BTPF, 3′-(3,5-bis(trifluoromethyl)-phenyl)-1′-(4-nitrophenyl)pyrazolino[70]fullerene),[47] and the ultrafast exciton relaxation, with reference to the 900 ps exciton lifetime of the neat DiO-PFDTBT film, was ascribed to the efficient quenching of excitons by the polymer-to-fullerene charge transfer reactions. In the present cases of PFDTBT/fullerene blends, the subpicosecond S_1 exciton lifetimes imply a nearly unitary quenching efficiency in viewing the 600 ps exciton lifetime of the neat PFDTBT film.

Parts a and b, respectively, of Figure 7 show the kinetics at λ_{pr} = 1000 nm plotted from the corresponding time-resolved spectra in Figures 3 and 4. (Figure S6 in the Supporting Information shows the 1000 nm kinetics recorded under λ_{ex} = 490 nm). The kinetics traces in part a or b of Figure 7 can be categorized into three different types. Type I comprises the kinetics traces of PFDTBT (neat) and PFDTBT/tris-PC_{61}BOE

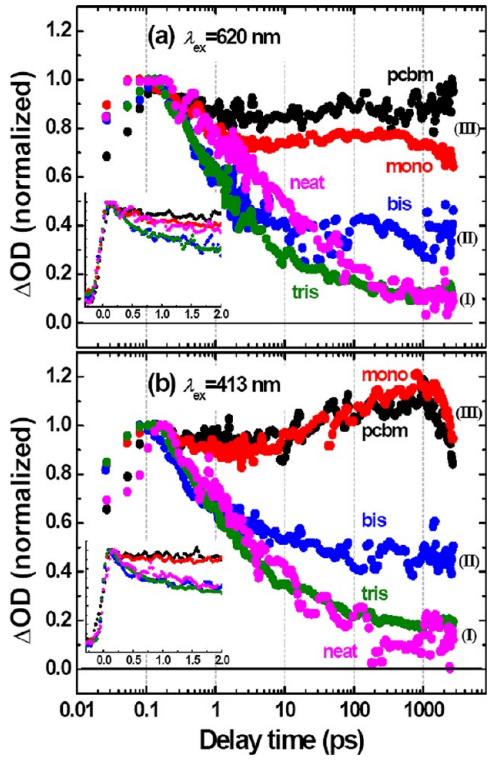

Figure 7. Kinetics up to 2.75 ns probed at 1000 nm for the neat and blend films (1:3, w/w) under the excitation wavelengths of (a) λ_{ex} = 620 nm and (b) λ_{ex} = 413 nm. The kinetics traces are normalized at 0.13 ps. Key: neat, PFDTBT; tris, PFDTBT/tris-PC_{61}BOE; bis, PFDTBT/bis-PC_{61}BOE; mono, PFDTBT/PC_{61}BOE; pcbm, PFDTBT/PC_{61}BM. The excitation photon fluence was (0.8−3.0) × 10^{13} photons·cm^{-2}·$pulse^{-1}$. See the text for details of the kinetics categorization (types I−III). The insets show the kinetics up to 2 ps in a linear abscissa for a clearer view of the initial decay phase.

(tris), which decay monotonically up to 100 ps and then proceed to a rather slow decay phase in the nanosecond regime. Type II refers to the kinetics of PFDTBT/bis-PC_{61}BOE (bis), which relaxes rapidly until 10 ps and, afterward, remains nearly constant. Type III consists of the kinetics of PFDTBT/mono-PC_{61}BOE (mono) and PFDTBT/PC_{61}BM (pcbm) evolving in a nonmonotonic manner: They relax slightly in 1 ps, rise until ∼1 ns, and decay again. These kinetics traces once again demonstrate the prominent influence of $-\Delta E_L$ on the dynamics of excitons and charge species to be interpreted in the Discussion.

We have examined the effects of the excitation photon fluence on the 1000 nm kinetics of the blends photoexcited at different wavelengths. As common features, within the initial 1 ps, the kinetics are independent of the excitation photon fluence, whereas after 1 ps they decay faster when the photon fluence becomes higher. For instance, in the case of PFDTBT/PC_{61}BM (Figure S7, Supporting Information), after the initial 1 ps decay that is independent of the photon fluence, the subsequent kinetics phase shows prominent photon fluence dependence, which can be ascribed to the nongeminate recombination of charge species. However, in the low-fluence regime of ∼10^{13} photons·cm^{-2}·$pulse^{-1}$, the kinetics are little affected by the photon fluence, which is a characteristic of the geminate charge recombination.

Figure 7 also shows the influence of the excitation wavelength on the kinetics. It is seen that shortening the

dx.doi.org/10.1021/jp308442t | J. Phys. Chem. C 2013, 117, 735−749

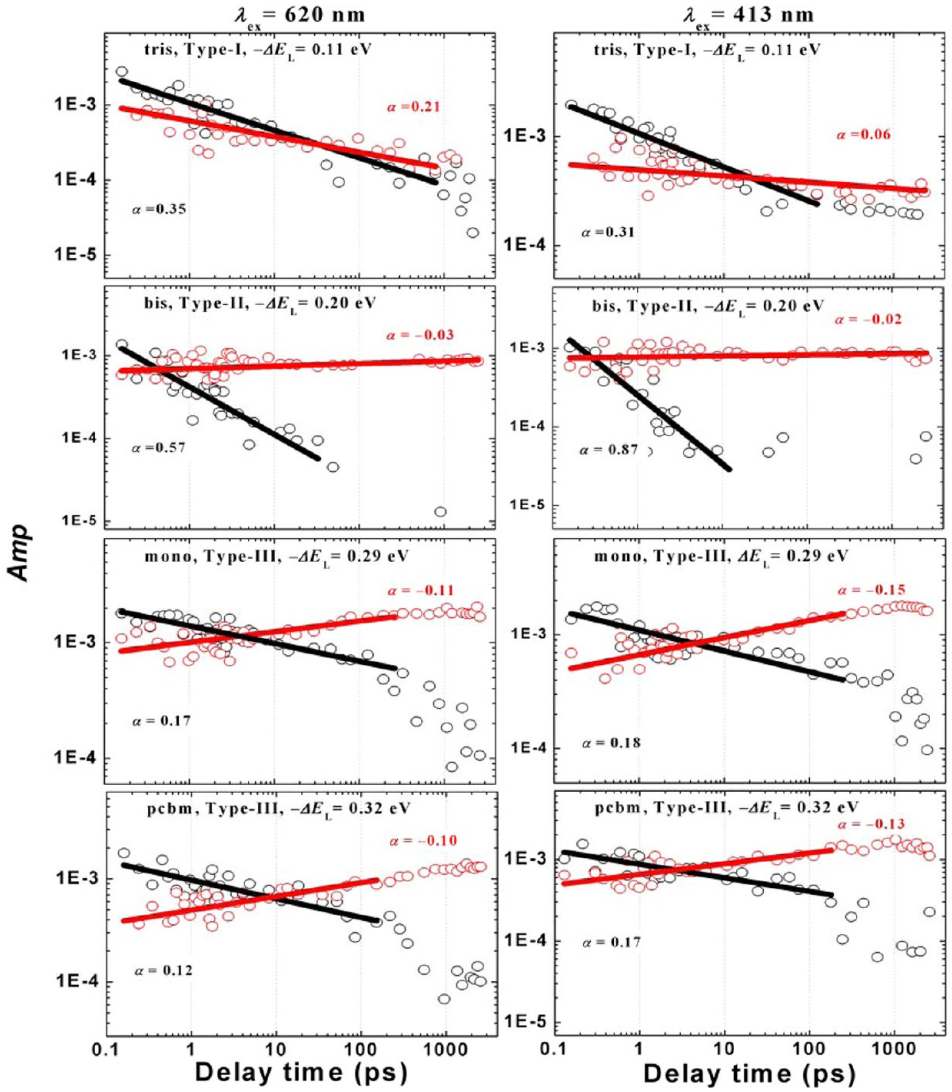

Figure 8. Log-to-log plots of time evolution profiles of ICT (black) and $P^{\bullet+}$ (red) for the blend films photoexcited at 620 nm (left panel) and 413 nm (right panel). Key: neat, PFDTBT; tris, PFDTBT/tris-PC_{61}BOE; bis, PFDTBT/bis-PC_{61}BOE; mono, PFDTBT/PC_{61}BOE, pcbm, PFDTBT/PC_{61}BM. The power law[71] Amp = $A_0(\Delta t^{-\alpha})$ was used to fit the linear sections of the kinetics traces, and resultant fitting curves are shown accordingly (solid lines).

excitation wavelength accelerates the decay of the type I kinetics and speeds up both the rise and the subsequent decay of the type III kinetics. The type III kinetics in Figure 7b are in excellent agreement with those of APFO3/PCBM photoexcited at 535 or 580 nm,[47,48] where the kinetics at 1000 nm were analyzed with a sequential model of charge photogeneration: S_1 + PCBM → $[e^-{:}h^+]$ followed by $[e^-{:}h^+]$ → e^- + h^+. The present work is intended to obtain the species-associated kinetics of the ICT ($[e^-{:}h^+]$) and CS states by decomposing the time-resolved spectra on the basis of the signature spectra in Figure 5a.

The species-associated kinetics of ICT and $P^{\bullet+}$ for the blend films are depicted in Figure 8. (Those at λ_{ex} = 490 nm are shown in Figure S8, Supporting Information.) In viewing the apparent log(Amp)-to-log(Δt) linear dependence, we fit the linear regions of the kinetics profiles to the power law log(Amp) = log(A_0) − α log(Δt), which is applicable to the characterization of the kinetics of charge species in energetically disordered organic photovoltaic materials.[72,73] The kinetics in Figure 8 are characterized as follows: (i) In general, upon shortening the excitation wavelength, the decay of ICT and decay/rise of $P^{\bullet+}$ become slightly faster, which is evident by comparing the slopes (α) in the left panel to those in the right panel. (ii) Regardless of the excitation wavelength, for PFDTBT/tris-PC_{61}BOE, the kinetics of ICT and $P^{\bullet+}$ (type I) decay monotonically over the entire delay time range, for PFDTBT/bis-PC_{61}BOE, the ICT kinetics (type II) decay steeply, whereas the polaron kinetics remain nearly constant, for PFDTBT/mono-PC_{61}BOE and PFDTBT/PC_{61}BM, the ICT kinetics (type III) decay with a slope of α = 0.12−0.18, while the polaron kinetics rise with α = −0.10 to −0.15. This apparent decay-to-rise correlation gets lost in the delay regime after ∼300 ps, and subsequently, the ICT state decays dramatically, while the polaron rises steadily to ∼1 ns. (iii) Importantly, the decay-to-rise correlation between the charge species, ICT and $P^{\bullet+}$, is observed merely for the type III kinetics with $-\Delta E_L$ above 0.2 eV, which is assigned to the ICT-to-CS conversion (vide infra). (iv) For all of the cases in Figure 8 the ICT states decay in a time frame of 10−1000 ps, in

dx.doi.org/10.1021/jp308442t | J. Phys. Chem. C 2013, 117, 735−749

agreement with the typical subnanosecond lifetimes of the ICT state reported for other polymer/fullerene systems.[42]

4. DISCUSSION

We now discuss the mechanism of charge photogeneration and role of the ICT state in yielding free charges. We will also examine the nature of the primary photoinduced species, the usage of $-\Delta E_L$ in driving the dissociation of the excitons and ICT states, and the influence of excess excitation and electrochemical energy on free charge generation. Before discussing these issues, we shall first discuss the mechanisms of charge photogeneration in the neat PFDTBT film, which may facilitate the understandings of the light conversion processes in the polymer/fullerene blends.

4.1. Mechanism of Charge Photogeneration in the Neat PFDTBT Film. In the TA spectra of neat PFDTBT films, the S_1 exciton dominates the spectral region around 1300 nm, while the interchain CT state and $P^{\bullet+}$ show up in the shorter wavelengths around 950 nm (Figures 3a and 4a). Except a 40 nm red shift of the absorption maximum, the interchain CT-state signature spectrum of the neat PFDTBT film is similar to the ICT spectra of the PFDTBT/fullerene blends (Figure S9, Supporting Information). The species-associated kinetics derived for the neat PFDTBT films are shown in Figure 9, on the basis of which we discuss the exciton and charge dynamics with reference to the scheme in Figure 10.

It is seen from Figure 9 that the interchain CT state appears immediately following the photoexcitation at 620 or 413 nm (Figure 10, path 2). $P^{\bullet+}$ appears simultaneously but merely

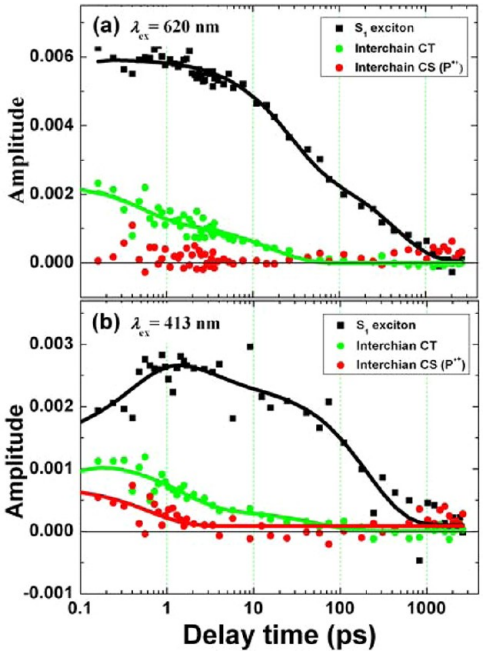

Figure 9. Species-associated kinetics of the S_1 exciton (black), interchain CT state (green), and CS state ($P^{\bullet+}$, red) for the neat PFDTBT films photoexcited at (a) 620 nm and (b) 413 nm. They were obtained by decomposing the TA spectral data sets (Figure S3, Supporting Information) according to $\Delta OD(\lambda,\Delta t) = Amp_0(\Delta t)\cdot exciton(\lambda) + Amp_1(\Delta t)\cdot CT(\lambda) + Amp_2(\Delta t)\cdot polaron(\lambda)$. Solid lines are fitting curves based on a multiexponential model function (see the Supporting Information, section S11, for the resultant time constants). The excitation photon fluence was 8.6×10^{12} photons·cm^{-2}·pulse^{-1}.

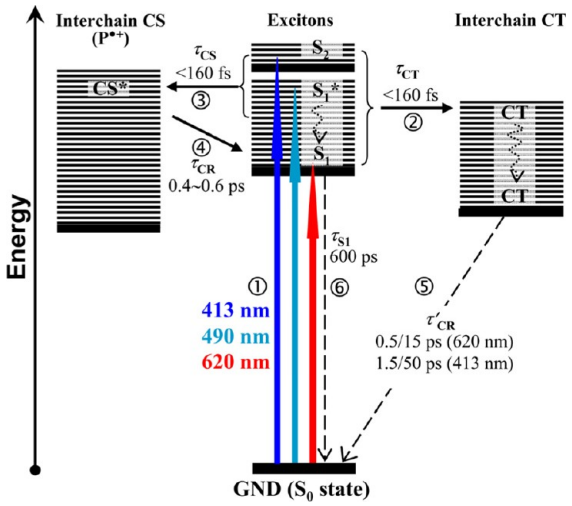

Figure 10. Excitation and charge photogeneration mechanisms proposed for the neat PFDTBT film. Relaxation of the exciton and interchain CT state are multiphasic. (Note the interchain characteristics of the CT and CS states.) The time scale of 160 fs is the fwhm of IRF.

under the above-gap photoexcitation (413 or 490 nm, Figure 10, path 3). Therefore, the S_2 and hot S_1 excitons (S_1*) can directly dissociate into $P^{\bullet+}$, but the relaxed S_1 exciton cannot. Curve fitting identified the biphasic exciton relaxation: 3.7 ps (20%) and 210 ps (80%) under the 413 nm excitation and 26 ps (50%) and 440 ps (50%) under the 620 nm excitation (Supporting Information, section S11). The considerably shortened exciton lifetimes upon higher photon energy excitation further prove that the excess excitation energy facilitates the dissociation of excitons. On the other hand, the interchain CT state relaxes with a pair of time constants of 0.5 and 15 ps (1.5 and 50 ps) under the photoexcitation at 620 nm (413 nm). Most importantly, the interchain CT state and $P^{\bullet+}$ decay independently, suggesting that the former is not a precursor of the latter. It is seen from Figure 9b that photoexcitation at 413 nm results in extremely short-lived $P^{\bullet+}$ with a decay time constant of 0.6 ± 0.1 ps, correlating closely to the rise of the exciton with a time constant of 0.4 ± 0.3 ps. The repopulation of excitons is also reflected by the corresponding spectral dynamics (Figure S3, Supporting Information): The TA transient at Δt = 0.68 ps becomes significantly stronger than the transient at Δt = 0.13 ps, which otherwise should be the strongest. We therefore conclude that the CS state recombines to the S_1 exciton in a subpicosecond time frame (Figure 10, path 4), whereas the interchain CT state recombines to the S_0 state in a few tens of picoseconds depending on the excitation wavelengths (Figure 10, path 5).

In the neat PCDTBT films, photogenerated mobile charges rather than neutral excitons had been suggested to be the primary species, which self-localize in ~100 fs and evolve to the bound S_1 excitons in less than 1 ps.[33] This view draws support from the decay-to-rise correlation between the CS state and the S_1 exciton observed in the present study, as well as from the lack of correlation between the exciton decay and the formation of the interchain CT state or CS state (Figure 9). However, judging from the amplitude ratios at Δt = 0.13 ps, the CS state and exciton, respectively, account for 15% and 50% of the overall primary excitation; that is, the neutral excitons rather than the CS states dominate the primary photoexcitation. This

dx.doi.org/10.1021/jp308442t | J. Phys. Chem. C 2013, 117, 735−749

is understandable because the ultrafast fluorescence detection in ref 33 could not simultaneously probe the emissive excitons and dark charge species. It is worth noting that the initial production of the interchain CT state, accounting for 25% of the overall photoexcitation, is independent of the excitation wavelength. Since the charge species, the interchain CT state and $P^{\bullet+}$, are identified with significant yields even before the time origin,[74] there is no doubt that they were generated within the IRF (160 fs). However, this does not necessarily mean that charge species are generated by direct photoexcitation, since the possibility that they are born from the S_1 exciton on an even shorter time scale cannot be excluded.

Charge formation and subsequent recombination are known to be important mechanisms responsible for the dramatic fluorescence quenching of polymers in the solid phase with reference to those in solution. In solution, photoinduced intermolecular charge transfer reaction in the π-stacked identical chromophores was previously reported for the dimers of 5PDI (1,7-bis(pyrrolidin-1′-yl)perylene-3,4:9,10-bis-(dicaboximide)), which was ascribed to the symmetry breaking of the singlet excited state.[75] This phenomenon is also documented for the special pairs of bacterial photosynthetic reaction centers.[76−78] In the same token, direct photogeneration of charge species in the neat PFDTBT film is considered to be an *interchain* process, which may take place in the ordered domains via symmetry breaking, or in the random phases owing to the energetic disorder with a typical magnitude of $\sigma \approx 0.1$ eV.[23] In both solid and solution phases PFDTBT shows rather similar ground-state absorption spectra. In addition, neat PFDTBT films do not give rise to discernible X-ray diffraction patterns (data not shown). Therefore, the PFDTBT molecules in the neat film may not be ordered enough to show significant crystallinity. In spite of this, PFDTBT molecules must be packed closely since significant yields of interchain charge states are photogenerated on an extremely short time scale. To summarize, the above-gap excitation generates $P^{\bullet+}$ with a yield of 15% and on a time scale comparable to the laser pulse duration, which recombines into the S_1 exciton in less than 1 ps. However, the band gap excitation (620 nm), not yielding any $P^{\bullet+}$, merely generates the interchain CT state. The excitation-wavelength-dependent formation of $P^{\bullet+}$ implies that in the neat PFDTBT film the excess energy deposited to excitons (S_1*, S_2) is essential for promoting the interchain charge separation reactions.

4.2. Mechanisms of Charge Photogeneraiton in PFDTBT/Fullerene Blends. The primary exciton and charge dynamics of the PFDTBT/fullerene blends differ distinctly from those of the neat films: (i) With respect to neat films, the initial quantum yields of the CS state and ICT state increase substantially. They are Φ_{CS} = 12−30% and Φ_{ICT} = 27−68% upon the photoexcitation at 620 nm and Φ_{CS} = 12−25% and Φ_{ICT} = 43−60% under shorter wavelength excitation at 413 nm (Supporting Information, section S12). Interestingly, the band gap photoexcitation at 620 nm, unable to induce the CS state in the neat PFDTBT film, yields a significant amount of CS states even for the PFDTBT/tris-PC_{61}BOE blend having a relatively small $-\Delta E_L$. This immediately points to the crucial role of the BHJ interface in boosting the efficiency of charge photogeneration. (ii) As seen from Figures 7 and 8, for PFDTBT mixed with bis-PC_{61}BOE, mono-PC_{61}BOE, and PC_{61}BM with $-\Delta E_L$ above 0.20 eV, the CS states live over nanoseconds (limited by the temporal detection window), whereas in the PFDTBT/tris-PC_{61}BOE blend with a relatively small $-\Delta E_L$ the CS state decays as fast as it does in the neat PFDTBT film (tens of picoseconds). (iii) In the cases of PFDTBT/mono-PC_{61}BOE and PFDTBT/PC_{61}BM, the ICT decay correlates intimately with the CS rise (Figure 8), which suggests that the ICT state is a precursor of the CS state.

On the basis of the results of spectral dynamics, species-associated kinetics, and exciton dissociation dynamics of the blend films, we propose the charge photogeneration mechanism for PFDTBT/PC_{61}BM as depicted in Figure 11, which is

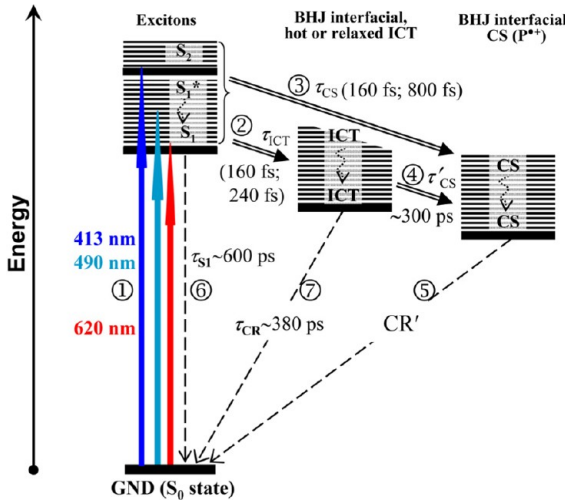

Figure 11. Proposed charge photogeneration mechanisms upon photoexcitation of the polymer for the PFDTBT/PC_{61}BM blend. Note that the ICT and CS states in the PFDTBT/fullerene blend are BHJ interfacial species and that upon higher photon energy excitation (413 nm) the contribution from fullerene excitation also comes into play,[84] which is not included here. The time scale of 160 fs is the fwhm of TRF. The time constant of the charge recombination process (5, CR′), ~30 ns, was previously reported in ref 48 for APFO3/PC_{61}BM.

also applicable to the PFDTBT/mono-PC_{61}BOE blend. First, we note that the interchain CT and CS states generated in bulk polymer domains contribute to the formation of the ICT and CS states, for which the BHJ interfaces provide the free energy driving force for the charges of opposite polarities to be separated.[79] As found for the neat PFDTBT film, the interchain CT and CS states appear on extremely short time scales (Figure 10, paths 2 and 3). Second, photoexcitation of PFDTBT creates S_1 or S_2 excitons, which subsequently convert into the ICT and CS states via polymer/fullerene interfacial charge transfer reactions (Figure 11, paths 2 and 3). We will comeback to this point in section 4.4. Furthermore, the ICT state further dissociates into the CS state on a time scale of ~300 ps (Figure 11, path 4) or returns to the ground state via charge recombination (~380 ps, Figure 11, path 7). Here, the time scale of ICT dissociation was obtained on the basis of the results of curve fittings to the species-associated kinetics of the CS rise ($\tau_r \approx 300$ ps) and ICT decay ($\tau_d \approx 160$ ps) for the PFDTBT/PCBM blend photoexcited at 620 nm (Figure 8), and the time scale of inherent ICT relaxation (~380 ps) was derived by assuming that the apparent ICT decay is due to the ICT-to-CS conversion (~300 ps) and charge recombination. The conversion time scale is considerably longer than that of a few tens of picoseconds derived for the APFO3/PCBM blends on the basis of model analyses of the ultrafast TA kinetics,[47,48] but it is comparable to the subnanosecond time scale recently observed for the P3HT/PC_{61}BM blends by means of the visible

dx.doi.org/10.1021/jp308442t | J. Phys. Chem. C 2013, 117, 735−749

pump−infrared probe vibrational spectroscopy.[85] Recent electro-optical pump−push experiments on working MDMO-PPV/$PC_{71}BM$ and PCPDTBT/$PC_{71}BM$ devices revealed the ultrafast (∼1 ps) cooling of the ICT states and a few percent photocurrent increase upon promotion of the relaxed ICT state to the hot ICT state by the near-infrared push pulses.[42] The ultrafast cooling of the ICT states seems to contradict the substantially slower ICT-to-CS conversion found in the present work. This may be due to the different natures of the initially prepared ICT states, an issue which deserves further investigation. Nevertheless, the $P^{\bullet+}$ photogeneration in the PFDTBT/$PC_{61}BM$ blend features a fast pathway and a delayed pathway in parallel, which were also found for other types of polymer/fullerene blends although the underlying mechanisms are different.[68,84] For example, in P3HT/$PC_{61}BM$ the 7−10 ps delayed formation of $P3HT^{\bullet+}$ was due to the exciton diffusion in the P3HT nanocrystallites.[68,79]

Our parallel mechanism differs from the sequential model of charge photogeneration suggested for APFO3 blended with $PC_{61}BM$, $PC_{71}BM$, or [70]BTPF,[47,48] and the discrepancy is explained below. In Figure 7b, the apparent decay in the initial 1 ps of the 1000 nm kinetics resembles closely that observed for APFO3/$PC_{61}BM$.[48] However, the assignment of this fast decay to exciton dissociation as made in ref 48 seems inappropriate: For PFDTBT/$PC_{61}BM$, the exciton almost completely decayed out at Δt = 0.13 ps as indicated by the rather small signature absorption over 1150−1350 nm (Figures 3 and 4). Therefore, the initial decay of the 1000 nm kinetics must be dominated by the charge species and hence should not be attributed to the exciton dissociation. To further clarify this issue, we have comparatively examined the kinetics at 900, 1000, and 1100 nm: The fast decay must be more prominent in the kinetics probed at longer wavelengths if it originates from exciton dissociation, which is indeed contradictory to the experimental observations (Figure S10, Supporting Information). Furthermore, in ref 48 the single kinetics trace at 1000 nm was analyzed on the basis of a sequential model, whereas in the present work the time-resolved spectra are analyzed on the basis of the signature spectra and species-associated kinetics without any analytical models being invoked. These together with the photon-fluence-independent decay of the 1000 nm kinetics (Figure S7, Supporting Information) lead us to propose that such initial decay is most likely due to ICT germinate recombination rather than exciton dissociation. Here, we note that the apparent initial decay in the 1000 nm kinetics is complicated by the processes of exciton splitting and charge formation/recombination and, therefore, by itself does not mean ultrafast charge recombination. The real decay kinetics are the species-associated ICT kinetics derived via spectral decomposition (Figure 8). In fact, the linear abscissa presentation of the 1000 nm kinetics in the insets of Figure 7 shows only a slight drop in the initial 1 ps for PFDTBT blended with $P_{61}CBM$ or mono-$PC_{61}BOE$ having a relatively large $-\Delta E_L$.

4.3. Roles of the ICT State in Free Charge Generation in PFDTBT/Fullerene Blends. The significant roles of the ICT state in free charge generation may be justified by the branching ratio between the parallel charge formation pathways, as well as by the competition between the ICT dissociation and recombination (Figure 11). For all of the PFDTBT/fullerene combinations in question, the initial yield of ICT is much higher than that of CS irrespective of the excitation wavelength. For instance, for the PFDTBT/$PC_{61}BM$ blend, the branching ratio Φ_{ICT}/Φ_{CS} = 3.4 under the photoexcitation at 620 nm decreases to 3.0 and 2.4 upon shortening of the excitation wavelengths to 490 and 413 nm, respectively (Supporting Information, section S12), implicitly meaning that the unrelaxed ICT state is prone to dissociate. On the other hand, the ICT dissociation rate, ∼300 ps^{-1}, is slightly higher than its recombination rate, 380 ps^{-1}, suggesting a dissociation efficiency exceeding 50%. For PFDTBT/bis-$PC_{61}BOE$ with $-\Delta E_L$ decreased to 0.20 eV, the time scale of ICT dissociation increases to 1 ns, implying a much lower dissociation efficiency. However, even in the case of PFDTBT/tris-$PC_{61}BOE$ with the $-\Delta E_L$ (0.11 eV) comparable to the energetic disorder of polymer films, a moderate quantum yield of overall charge production, $\Phi_{ICT} + \Phi_{CS}$ = 40−50%, was observed. Nevertheless, given a sufficiently large $-\Delta E_L$, the ICT state plays a crucial role in yielding free charges owing to the high ICT-to-CS branching ratio and efficient ICT-to-CS dissociation. Our results show that, with $-\Delta E_L \approx 0.3$ eV the total yield of charge species ($\Phi_{ICT} + \Phi_{CS}$) is 85−90% irrespective of the excitation wavelength (Supporting Information, section S12), in accordance with the 70−80% internal quantum efficiency of the PFDTBT/$PC_{71}BM$ device.[58] In this context, recent investigations have suggested that under the device operating conditions the built-in electrical fields can further promote the ICT dissociation, which in competition with its recombination highly influence the $I-V$ characteristics.[42,50,80,81] Here, we note that both the branching ratio and the ICT-to-CS conversion efficiency can be dependent on the film morphologies of polymer/fullerene blends, which may partially explain the rather low ICT-to-CS branching ratio of 1:9 reported for the PCDTBT/fullerene blends.[52]

4.4. Driving Force for Interfacial Charge Transfer Reaction: $-\Delta E_L$ Influence on ICT Dissociation. We now discuss how the $-\Delta E_L$ is utilized to drive the conversion of the exciton to CS and ICT states via interfacial charge transfer reactions and to promote the dissociation of ICT into CS in a blend film. It is noteworthy that Marcus's theory is viable for the definite single-step electron transfer reactions.[59] Therefore, within this theoretical framework different electron transfer pathways established above have to be examined separately. The systematically tuned $-\Delta E_L$ and its significant influence on the species-associated kinetics provide us with a unique opportunity to clarify these issues. In the following discussion on the mechanisms of interfacial charge transfer and dissociation, we shall confine ourselves to consider the case of band gap excitation (620 nm). Thus, the primary excitations mainly comprise the S_1 exciton and interchain CT state in the bulk polymer domain, which will be collectively referred to as the exciton. In addition, we shall examine the excitation and charge processes in the initial subpicosecond regime so as to minimize the influence from multistep processes.

According to the recent work of Durrant and co-workers,[23,27] the free energy driving force (ΔG°_{CS}) for exciton-to-CS charge transfer is defined as the energy difference between the exciton and CS states. The CS-state energy is estimated from the difference between the ionization potential of the donor (IP_D) and the electron affinity of the acceptor (EA_A). Thus, we have $\Delta G^\circ_{CS} = E_{ex} - (IP_D - EA_A)$, where E_{ex} denotes the state energy of the exciton. By approximating IP_D and EA_A to the electrochemically determined HOMO energy of the polymer (D) and LUMO energy of fullerene (A), respectively, the driving force can be related directly to the fullerene/polymer LUMO level offset ($\Delta G^\circ_{CS} = \Delta E_L$).

dx.doi.org/10.1021/jp308442t | J. Phys. Chem. C 2013, 117, 735−749

We have determined the initial polaron yields at Δt = 0.13 ps ($[P^{\bullet+}]_{0.13ps}$) from the species-associated kinetics (Figure 8). The ln $[P^{\bullet+}]_{0.13ps}$ to $-\Delta G^{\circ}_{CS}$ plot turns out to be a parabola (Figure 12a). In addition, we have derived the individual ICT

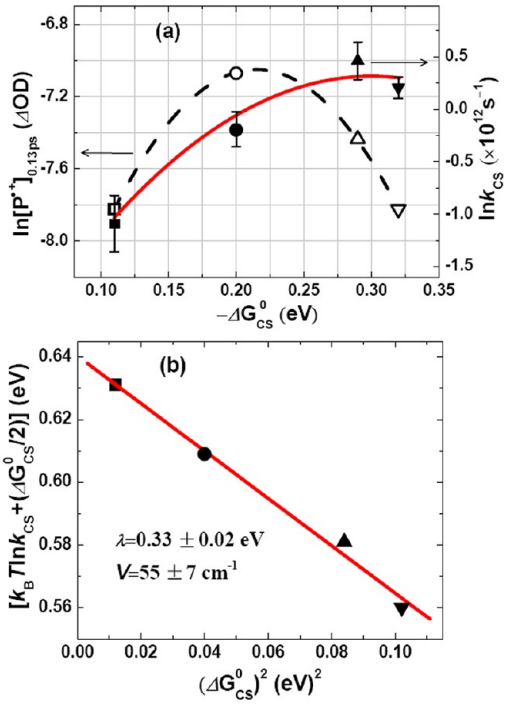

Figure 12. (a) Exciton-to-CS charge transfer rate (k_{CS}, filled symbols) and polaron production at Δt = 0.13 ps ($[P^{\bullet+}]_{0.13ps}$, open symbols) against $-\Delta G^{\circ}_{CS}(-\Delta E_L)$. Solid lines are obtained by fitting the individual data set to a parabolic model function. Data points are for PFDTBT mixed with tris-PC_{61}BOE (□/■), bis-PC_{61}BOE (○/●), mono-PC_{61}BOE (Δ/▲), and PC_{61}BM (∇/▼). The blend films were photoexcited at 620 nm with a photon fluence of 9.1 × 10^{12} photons·cm^{-2}·$pulse^{-1}$. (b) k_BT ln k_{CS} + $\Delta G^{\circ}_{CS}/2$ against $(\Delta G^{\circ}_{CS})^2$, for which ΔE_L is used to approximate ΔG°_{CS}. The indicated coupling strength (V) and reorganization energy (λ), respectively, are derived from the intercept and slope (see the text for details).

and CS formation rates (k_{ICT} and k_{CS}) from the overall exciton dissociation rates (Figure 6, $k = k_{ICT} + k_{CS}$) and ratios of the initial quantum yields (Φ_{ICT}:Φ_{CS}, Supporting Information, section S12). The ln k_{CS} to $-\Delta G^{\circ}_{CS}$ plot also appears as a parabola (Figure 12a). Note that the time scale of exciton-to-ICT conversion is k_{ICT}^{-1} = 240 fs and, to our surprise, that of exciton-to-CS conversion is k_{CS}^{-1} = 820 fs (Figure 11, paths 2 and 3). Nevertheless, these parabolic relations strongly suggest that the exciton-to-CS transition obeys Marcus's nonadiabetic electron transfer mechanism:[55,59]

$$k_{CS} = \left(\frac{4\pi^3}{h^2\lambda k_B T}\right)^{1/2} V^2 \exp\left[-\frac{(\Delta G^{\circ}_{CS} + \lambda)^2}{4\lambda k_B T}\right] \quad (1)$$

where h is Planck's constant, and V and λ, respectively, represent the electronic coupling strength and total reorganization energy, which can be determined from the Marcus plot[55]

$$k_B T \ln k_{CS} + \frac{\Delta G^{\circ}_{CS}}{2} = k_B T \ln\left[\left(\frac{4\pi^3}{h^2\lambda k_B T}\right)^{1/2} V^2\right] - \frac{\lambda}{4} - \frac{(\Delta G^{\circ}_{CS})^2}{4\lambda} \quad (2)$$

Equation 2 allows us to derive V = 55 ± 7 cm^{-1} and λ = 0.33 ± 0.02 eV, respectively, from the intercept and slope of the Marcus plot (Figure 12b). The nice linearity of the Marcus plot suggests that the variation in k_{CS} is governed by $\Delta G^{\circ}_{CS}(\Delta E_L)$. However, on going from mono- to trissubstituted fullerenes, the influence of the polymer/fullerene interfacial morphology on k_{CS} cannot be completely excluded. The λ value of 0.33 eV is not too far from the intermolecular reorganization energy of ZnP-ref/C_{60}-ref (0.47 eV)[55] and poly(9,9-dioctylfluorene)/fullerene (0.4 eV).[82] Since the activation energy (ΔG^*) of an electron transfer reaction follows $\Delta G^* = (\Delta G^{\circ}_{CS} + \lambda)^2/\lambda$, the $-\Delta G^{\circ}_{CS}$ for barrierless exciton-to-CS charge transfer turns out to be 0.33 eV. In this context, efficient charge photogeneration was observed for the PCPDTBT/PCBM blend with a considerably small $-\Delta G^{\circ}_{CS}$ of 0.1 eV, which is suggestive of specific molecular interactions.[10,37]

For PFDTBT/PC_{61}BM and PFDTBT/mono-PC_{61}BOE with relatively larger $-\Delta E_L$ values, the species-associated kinetics in Figure 8a show tight decay-to-rise correlation between the ICT and CS states, suggesting the transformation of ICT into $P^{\bullet+}$. In contrast, for PFDTBT/tris-PC_{61}BOE and PFDTBT/bis-PC_{61}BOE with relatively small $-\Delta E_L$ values, the kinetics of ICT and CS evolve independently, implying that the ICT state cannot effectively dissociate into the CS state. To better understand the precursors and mechanisms of $P^{\bullet+}$ production, we now examine the charge yield $[P^{\bullet+}]_{2ns}$ defined as the $P^{\bullet+}$ amplitude at Δt = 2 ns (Figure 8). Figure 13a shows the $-\Delta E_L$ dependence of the overall yield $[P^{\bullet+}]_{2ns}$ and that of the contribution of ICT dissociation in the 0.13 ps to 2 ns temporal regime, $[P^{\bullet+}]_{2ns}-[P^{\bullet+}]_{0.13ps}$. It is seen that the $[P^{\bullet+}]_{2ns}-[P^{\bullet+}]_{0.13ps}$ curve rises rapidly on $-\Delta E_L$ exceeding 0.2 eV, indicating that the ICT dissociation also relies intimately on the chemical potential difference at the BHJ interfaces.

In Figure 13b, it is seen that the rate of ICT formation, ln k_{ICT}, increases monotonically upon $-\Delta E_L$ being increased from 0.11 to 0.32 eV. Here, it is reasonable to assume that ICT forms via charge transfer at the polymer/fullerene interfaces following Marcus's electron transfer mechanism. Unfortunately, the rather scattered data points impair the quantities V and λ from being derived as we did for the exciton-to-CS charge transfer reactions. Nevertheless, in comparison to the parabolic behavior of ln k_{CS} or $[P^{\bullet+}]_{0.13ps}$ (Figure 12a), it seems that the apex of the ln k_{ICT} plot appears at a larger $-\Delta E_L$; i.e., the reorganization energy of exciton-to-ICT interfacial charge transfer may be larger than that of exciton-to-CS interfacial charge transfer. The above discussion suggests that both exciton-to-CS and exciton-to-ICT conversions obey Marcus's nonadiabetic electron transfer mechanism. Hereafter, we will show that the ICT-to-CS conversion can be well accounted for by Braun−Onsager's escape probability for a coupled e^-−h^+ pair in disordered solid media.

As seen from Figure 13, a larger $-\Delta E_L$ leads to a higher overall polaron production $[P^{\bullet+}]_{2ns}$, a tendency which is in accordance with the e^-−h^+ escape probability ($P(a)$) in the absence of an electronic field,[23,27,60] $P(a) = \exp(-r_c/a)$, where r_c stands for the Coulomb capture radius estimated to be 4 nm

dx.doi.org/10.1021/jp308442t | J. Phys. Chem. C 2013, 117, 735−749

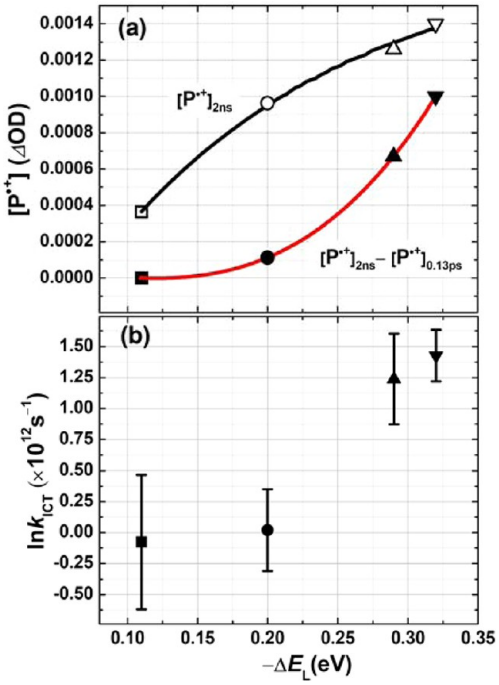

Figure 13. (a) Polaron production at Δt = 2 ns ($[P^{\bullet+}]_{2ns}$, open symbols) and neat contribution of ICT dissociation ($[P^{\bullet+}]_{2ns}-[P^{\bullet+}]_{0.13ps}$, filled symbols) against $-\Delta E_L$. Solid lines are for guiding the eyes. (b) ICT formation rate (k_{ICT}) vs $-\Delta E_L$. The blends were photoexcited at λ_{ex} = 620 nm under a photon fluence of 9.1 × 10^{12} photons·cm^{-2}·$pulse^{-1}$. Data points are for PFDTBT mixed with tris-PC_{61}BOE (□/■), bis-PC_{61}BOE (○/●), mono-PC_{61}BOE (Δ/▲), and PC_{61}BM (∇/▼).

assuming an ε_r of 3.5 and an effective Coulomb binding energy of 0.1 eV,[23,28] and a refers to the thermalization length (initial e^-–h^+ separation). It appears that the $-\Delta E_L$ dependence of $[P^{\bullet+}]_{2ns}$ agrees well with the a dependence of $P(a)$ (see the Supporting Information, section S13), suggesting that the influence of $-\Delta E_L$ on polaron production can be virtually translated into its effect on the initial e^-–h^+ separation; that is, a larger $-\Delta E_L$ leads to a larger e^-–h^+ separation. To gain an impression, it is roughly estimated that an $-\Delta E_L$ of 0.11–0.32 eV corresponds to an initial e^-–h^+ separation of 4–11 nm (Supporting Information, section S13). Here, we note the important role of ICT dissociation in yielding free charges: When direct exciton-to-CS charge transfer falls into Marcus's inverted region ($-\Delta E_L$ > 0.3 eV), free charge production via Braun–Onsager's e^-–h^+ escape mechanism becomes predominant.

Finally, we comment on the effects of excess energy on the ICT dissociation efficiency defined by $([P^{\bullet+}]_{2ns}-[P^{\bullet+}]_{0.13ps})/[ICT]_{0.13ps}$. The results in Figure 14 demonstrate a rapid increase of ICT-to-CS conversion efficiency with increasing $-\Delta E_L$. Compared to the increase of the excitation photon energy, the increase of $-\Delta E_L$ is much more effective for a higher conversion efficiency. Here, the chemical potential, $-\Delta E_L$, provides excess energy of ICT, in analogy to the excitation photon energy supplying excess energy of excitons. The relatively weaker effect of the photon energy is in accordance with the recent finding that efficient ICT dissociation does not need large exciton-associated excess energy.[42,83] However, it is interesting to see the synergistic effect of the photon energy and $-\Delta E_L$ in accelerating the ICT

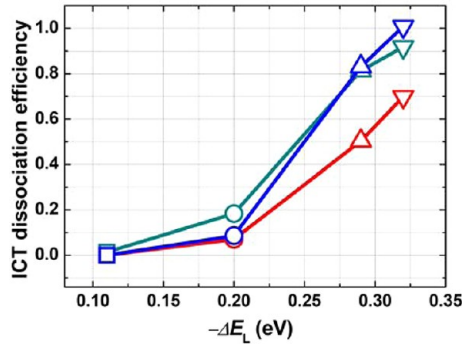

Figure 14. Photon energy dependence of the ICT dissociation efficiency defined by $([P^{\bullet+}]_{2ns}-[P^{\bullet+}]_{0.13ps})/[ICT]_{0.13ps}$ under the excitation wavelengths of 620 nm (red), 490 nm (cyanine), and 413 nm (blue). Key: PFDTBT/tris-PC_{61}BOE (□), PFDTBT/bis-PC_{61}BOE (○), PFDTBT/mono-PC_{61}BOE (Δ) and PFDTBT/PC_{61}BM (∇).

dissociation. On the other hand, the rise of the efficiency curve under 413 nm excitation is evidently faster than that under longer wavelength excitations, which is ascribable to the contribution of fullerene excitations.[84] Importantly, by comparing the ICT conversion efficiency under 620 nm excitation to those under higher photon energy excitations, we see that the narrow-band-gap copolymers can efficiently harvest and convert near-infrared light into free charges provided a large enough $-\Delta E_L$ (>0.2 eV).

5. SUMMARY

We have investigated the primary exciton and charge dynamics of the neat PFDTBT and PFDTBT/fullerene films with systematic tuning of $-\Delta E_L$ over 110–320 meV (corresponding to 4–13 k_BT). Examining the influence of $-\Delta E_L$ on the species-associated ultrafast dynamics of the S_1 exciton and charge species (ICT and CS) allows us to verify the detailed mechanisms of charge photogeneration, as well as the role of ICT in yielding free charge. The spectroscopic data obtained with low-fluence photoexcitation and near-infrared detection combined with the model-independent analyses give rise to deeper insights into a number of crucial issues reconsolidated below.

For the neat PFDTBT film (cf. Figure 10), the above-gap photoexcitaiton generates the *interchain* CT and CS states with an overall yield (Φ_{CT} + Φ_{CS}) of ~40%. However, the band gap photoexcitation merely produces the interchain CT state (Φ_{CT} ≈ 25%), which recombines biphasically with time constants of 0.5 and 15 ps. Upon the above-gap excitation, the CS state relaxes into the S_1 exciton with a time constant of 0.4–0.6 ps, which is supportive of the view that charges can be the primary excitation forms.[32,33] However, we show that half of the primary excitations are neutral excitons whereas the CS yield is only 15%.

For the PFDTBT/fullerene blends (cf. Figure 11), polymer photoexcitation generates the ICT and CS states in a parallel manner irrespective of the excitation wavelength, which redresses the sequential model previously suggested for the same type of copolymers.[47,48] Our parallel model is in accordance with that proposed for the PCDTBT/fullerene blends,[32,35] although therein the issue of ICT-to-CS conversion (Figure 11, path 4) remained unclear. Meanwhile, the present work proves that the ICT state acts as either a trap or a precursor of free charges depending on the size of $-\Delta E_L$. It can

dx.doi.org/10.1021/jp308442t | J. Phys. Chem. C 2013, 117, 735–749

dissociate into the CS state provided a sufficiently large $-\Delta E_L$. For example, for $-\Delta E_L$ above 0.30 eV as in the case of PFDTBT/$PC_{61}BM$, the ICT-to-CS conversion efficiency exceeds 50%, which together with the large ICT-to-CS branching ratio (3:1) manifests the crucial role of ICT in yielding free charges.

The exciton-to-CS charge transfer reaction (Figure 11, path 3) can be well accounted for by Marcus's nonadiabetic electron transfer theory with a reorganization energy of 0.33 ± 0.02 eV and a coupling strength of 55 ± 7 cm^{-1}. To our surprise, this path accounts for only 10−25% of the overall charge production given an ICT-to-CS partition of ∼3:1, and for $-\Delta E_L$ exceeding 0.33 eV the reaction efficiency starts to decrease as it switches into the Marcus inverted region. Thus, an $-\Delta E_L$ of 0.33 eV ensures both barrierless exciton-to-CS charge transfer and efficient ICT-to-CS conversion, which may be important in guiding the energetics optimization for photovoltaic materials.

Our ultrafast spectroscopic results suggest that, for the PFDTBT/fullerene blends with $-\Delta E_L$ exceeding 0.20 eV, the ICT dissociation (Figure 11, path 4) starts to dominate the free charge production. This process can be accounted for by Braun−Osager's model of e^-−h^+ dissociation, showing that a larger initial e^-−h^+ separation of the ICT state leads to a higher dissociation probability. It had been shown that the electron delocalization length is highly dependent on the topology and bulkiness of the acceptor molecules,[85] while the hole delocalization relies on the molecular structures of polymers,[42] both of which are considered to be crucial for free charge generation via ICT dissociation. On the other hand, a variety of initial e^-−h^+ separations are expected at a given chemical potential $-\Delta E_L$ in view of the fact that both polymer and fullerenes are agglomerated to different degrees.[86,87] Therefore, optimization of the phase separation of the blends and molecular structures of polymers to support large extents of primary charge delocalization are worthy of continuing efforts to further improve the device performance.

■ ASSOCIATED CONTENT

Supporting Information

Cyclic voltammograms, characteristic polaron absorption, exciton lifetimes, additional TA spectra and kinetics, quantum yields of the exciton and charge species, and comparison of free charge production to the model prediction. This material is available free of charge via the Internet at http://pubs.acs.org.

■ AUTHOR INFORMATION

Corresponding Author

*Phone: +86-10-62516604. Fax: +86-10-62516444. E-mail: jpzhang@chem.ruc.edu.cn (J.-P.Z.); hjhzlz@iccas.ac.cn (J.-H.H.).

Notes

The authors declare no competing financial interest.

■ ACKNOWLEDGMENTS

Grants in aid from the Natural Science Foundation of China (20933010, 21133001, and 51173189) and National Basic Research Program of China (2009CB20008) are acknowledged. We are grateful for support from the Fundamental Research Funds for the Central Universities and Research Funds of the Renmin University of China (Grant 10XNI007).

■ REFERENCES

(1) Yu, G.; Gao, J.; Hummelen, J. C.; Wudl, F.; Heeger, A. J. *Science* **1995**, *270*, 1789−1791.
(2) He, Z.; Zhong, C.; Huang, X.; Wong, W.-Y.; Wu, H.; Chen, L.; Su, S.; Cao, Y. *Adv. Mater.* **2011**, *23*, 4636−4643.
(3) Green, M. A.; Emery, K.; Hishikawa, Y.; Warta, W. *Prog. Photovoltaics: Res. Appl.* **2011**, *19*, 84−92.
(4) Chen, H. Y.; Hou, J.; Zhang, S.; Liang, Y.; Yang, G.; Yang, Y.; Yu, L.; Wu, Y.; Li, G. *Nat. Photonics* **2009**, *3*, 649−653.
(5) Liang, Y.; Yu, L. *Acc. Chem. Res.* **2010**, *43*, 1227−1236.
(6) Liang, Y.; Xu, Z.; Xia, J.; Tsai, S.-T.; Wu, Y.; Li, G.; Ray, C.; Yu, L. *Adv. Mater.* **2010**, *22*, E135−E138.
(7) Zhou, H.; Yang, L.; Stuart, A. C.; Price, S. C.; Liu, S.; You, W. *Angew. Chem., Int. Ed.* **2011**, *50*, 2995−2998.
(8) Chu, T.-Y.; Lu, J.; Beaupré, S.; Zhang, Y.; Pouliot, J.-R.; Wakim, S.; Zhou, J.; Leclerc, M.; Li, Z.; Ding, J.; et al. *J. Am. Chem. Soc.* **2011**, *133*, 4250−4253.
(9) Dennler, G.; Scharber, M. C.; Brabec, C. J. *Adv. Mater.* **2009**, *21*, 1323−1338.
(10) Peet, J.; Kim, J. Y.; Coates, N. E.; Ma, W. L.; Moses, D.; Heeger, A. J.; Bazan, G. C. *Nat. Mater.* **2007**, *6*, 497−500.
(11) Lenes, M.; Wetzelaer, G.-J. A. H.; Kooist, F. B.; Veenstra, S. C.; Hummelen, J. C.; Blom, P. W. M. *Adv. Mater.* **2008**, *20*, 2116−2119.
(12) Zhao, G.; He, Y.; Li, Y. *Adv. Mater.* **2010**, *22*, 4355−4358.
(13) Yang, C.; Kim, J. Y.; Cho, S.; Lee, J. K.; Heeger, A. J.; Wudl, F. *J. Am. Chem. Soc.* **2008**, *130*, 6444−6450.
(14) Wienk, M. M.; Kroon, J. M.; Verhees, W. J. H.; Knol, J.; Hummelen, J. C.; van Hal, P. A.; Janssen, R. A. J. *Angew. Chem., Int. Ed.* **2003**, *42*, 3371−3375.
(15) Ma, W.; Yang, C.; Gong, X.; Lee, K.; Heeger, A. J. *Adv. Funct. Mater.* **2005**, *15*, 1617−1622.
(16) Kim, Y.; Cook, S.; Tuladhar, S. M.; Choulis, S. A.; Nelson, J.; Durrant, J. R.; Bradley, D. D. C.; Giles, M.; Mcculloch, I.; Ha, C.-S.; et al. *Nat. Mater.* **2006**, *5*, 197−203.
(17) Erb, T.; Zhokhavets, U.; Gobsch, G.; Raleva, S.; Stühn, B.; Schilinsky, P.; Waldauf, C.; Brabec, C. J. *Adv. Funct. Mater.* **2005**, *15*, 1193−1196.
(18) Li, G.; Shrotriya, V.; Huang, J.; Yao, Y.; Moriarty, T.; Emery, K.; Yang, Y. *Nat. Mater.* **2005**, *4*, 864−868.
(19) Chen, W.; Xu, T.; He, F.; Wang, W.; Wang, C.; Strzalka, J.; Liu, Y.; Wen, J.; Miller, D. J.; Chen, J.; et al. *Nano Lett.* **2011**, *11*, 3707−3713.
(20) Seo, J. H.; Gutacker, A.; Sun, Y.; Wu, H.; Huang, F.; Cao, Y.; Scherf, U.; Heeger, A. J.; Bazan, G. C. *J. Am. Chem. Soc.* **2011**, *133*, 8416−8419.
(21) Kim, J. Y.; Lee, K.; Coates, N. E.; Moses, D.; Nguyen, T.-Q.; Dante, M.; Heeger, A. J. *Science* **2007**, *317*, 222−225.
(22) Dou, L.; You, J.; Yang, J.; Chen, C.-C.; He, Y.; Murase, S.; Moriarty, T.; Emery, K.; Li, G.; Yang, Y. *Nat. Photonics* **2012**, *6*, 180−185.
(23) Clarke, T. M.; Durrant, J. R. *Chem. Rev.* **2010**, *110*, 6736−6767.
(24) Deibel, C.; Dyakonov, V. *Rep. Prog. Phys.* **2010**, *73*, 096401.
(25) Brabec, C. J.; Sariciftci, N. S.; Hummelen, J. C. *Adv. Funct. Mater.* **2001**, *11*, 15−26.
(26) Persson, N.-K.; Arwin, H.; Inganas, O. *J. Appl. Phys.* **2005**, *97*, 034503.
(27) Ohkita, H.; Cook, S.; Astuti, Y.; Duffy, W.; Tierney, S.; Zhang, W.; Heeney, M.; McCulloch, I.; Nelson, J.; Bradley, D. D. C.; Durrant, J. R. *J. Am. Chem. Soc.* **2008**, *130*, 3030−3042.
(28) de Haas, M. P.; Warman, J. M.; Anthopoulos, T. D.; de Leeuw, D. M. *Adv. Funct. Mater.* **2006**, *16*, 2274−2280.
(29) Deibel, C.; Mack, D.; Gorenflot, J.; Schöll, A.; Krause, S.; Reinert, F.; Rauh, D.; Dyakonov, V. *Phys. Rev. B* **2010**, *81*, 085202.
(30) Piliego, C.; Loi, M. A. *J. Mater. Chem.* **2012**, *22*, 4141−4150.
(31) Faist, M. A.; Kirchartz, T.; Gong, W.; Ashraf, R. S.; McCulloch, I.; de Mello, J. C.; Ekins-Daukes, N. J.; Bradley, D. D. C.; Nelson, J. *J. Am. Chem. Soc.* **2012**, *134*, 685−692.
(32) Tong, M.; Coates, N. E.; Moses, D.; Heeger, A. J. *Phys. Rev. B* **2010**, *81*, 125210.

(33) Banerji, N.; Cowan, S.; Leclerc, M.; Vauthey, E.; Heeger, A. J. *J. Am. Chem. Soc.* **2010**, *132*, 17459−17470.
(34) Halls, J. J. M.; Cornil, J.; dos Santos, D. A.; Silbey, R.; Hwang, D.-H.; Holmes, A. B.; Brédas, J. L.; Friend, R. H. *Phys. Rev. B* **1999**, *60*, 5721−5727.
(35) Brédas, J.; Beljonne, D.; Coropceanu, V.; Cornil, J. *Chem. Rev.* **2004**, *104*, 4971−5003.
(36) Pensack, R. D.; Asbury, J. B. *J. Phys. Chem. Lett.* **2010**, *1*, 2255−2263.
(37) Clarke, T.; Ballantyne, A.; Jamieson, F.; Brabec, C.; Nelson, J.; Durrant, J. *Chem. Commun.* **2009**, 89−91.
(38) Shoaee, S.; An, Z.; Zhang, X.; Barlow, S.; Marder, S. R.; Duffy, W.; Heeney, M.; McCulloch, I.; Durrant, J. R. *Chem. Commun.* **2009**, 5445−5447.
(39) Clarke, T. M.; Ballantyne, A. M.; Tierney, S.; Heeney, M.; Duffy, W.; McCulloch, I.; Nelson, J.; Durrant, J. R. *J. Phys. Chem. C* **2010**, *114*, 8068−8075.
(40) Shoaee, S.; Clarke, T. M.; Huang, C.; Barlow, S.; Marder, S. R.; Heeney, M.; McCulloch, I.; Durrant, J. R. *J. Am. Chem. Soc.* **2010**, *132*, 12919−12926.
(41) Veldman, D.; Meskers, S. C. J.; Janssen, R. A. J. *Adv. Funct. Mater.* **2009**, *19*, 1939−1948.
(42) Bakulin, A. A.; Rao, A.; Pavelyev, V. G.; van Loosdrecht, P. H. M.; Pshenichnikov, M. S.; Niedzialek, D.; Cornil, J.; Beljonne, D.; Friend, R. H. *Science* **2012**, *335*, 1340−1344.
(43) Goris, L.; Haenen, K.; Nesládek, M.; Wagner, P.; Vanderzande, D.; de Schepper, L.; D'haen, J.; Lutsen, L.; Manca, J. V. *J. Mater. Sci.* **2005**, *40*, 1413−1418.
(44) Holcombe, T. W.; Norton, J. E.; Rivnay, J.; Woo, C. H.; Goris, L.; Piliego, C.; Griffini, G.; Sellinger, A.; Brédas, J.-L.; Salleo, A.; et al. *J. Am. Chem. Soc.* **2011**, *133*, 12106−12114.
(45) Loi, M. A.; Toffanin, S.; Muccini, M.; Forster, M.; Scherf, U.; Scharber, M. *Adv. Funct. Mater.* **2007**, *17*, 2111−2116.
(46) Vandewal, K.; Gadisa, A.; Oosterbaan, W. D.; Bertho, S.; Banishoeib, F.; Van Severen, I.; Lutsen, L.; Cleij, T. J.; Vanderzande, D.; Manca, J. V. *Adv. Funct. Mater.* **2008**, *18*, 2064−2070.
(47) Pal, S. K.; Kesti, T.; Maiti, M.; Zhang, F.; Inganäs, O.; Hellström, S.; Andersson, M. R.; Oswald, F.; Langa, F.; Österman, T.; et al. *J. Am. Chem. Soc.* **2010**, *132*, 12440−12451.
(48) De, S.; Pascher, T.; Maiti, M.; Jespersen, K. G.; Kesti, T.; Zhang, F.; Inganäs, O.; Yartsev, A.; Sundström, V. *J. Am. Chem. Soc.* **2007**, *129*, 8466−8472.
(49) Muntwiler, M.; Yang, Q.; Tisdale, W. A.; Zhu, X.-Y. *Phys. Rev. Lett.* **2008**, *101*, 196403.
(50) Friend, R. H.; Phillips, M.; Rao, A.; Wilson, M. W. B.; Li, Z.; McNeill, C. R. *Faraday Discuss.* **2012**, *155*, 339−348.
(51) APFO3 is also abbreviated as Dio-PFDTBT, and it differs from BisDMO-PFDTBT of the present work only in the alkyl side chains.
(52) Etzold, F.; Howard, I. A.; Mauer, R.; Meister, M.; Kim, T.-D.; Lee, K.-S.; Baek, N. S.; Laquai, F. *J. Am. Chem. Soc.* **2011**, *133*, 9469−9479.
(53) Gulbinas, V.; Hertel, D.; Yartsev, A.; Sundström, V. *Phys. Rev. B* **2007**, *76*, 235203.
(54) Müller, J. G.; Lupton, J. M.; Feldmann, J.; Lemmer, U.; Scharber, M. C.; Sariciftci, N. S.; Brabec, C. J.; Scherf, U. *Phys. Rev. B* **2005**, *72*, 195208.
(55) Imahori, H.; Yamada, H.; Guldi, D. M.; Endo, Y.; Shimomura, A.; Kundu, S.; Yamada, K.; Okada, T.; Sakata, Y.; Fukuzumi, S. *Angew. Chem., Int. Ed.* **2002**, *41*, 2344−2347.
(56) Lane, P. A.; Wei, X.; Vardeny, Z. V. *Phys. Rev. B* **1997**, *56*, 4626−4637.
(57) Svensson, M.; Zhang, F.; Veenstra, S. C.; Verhees, W. J. H.; Hummelen, J. C.; Kroon, J. M.; Inganäs, O.; Andersson, M. R. *Adv. Mater.* **2003**, *15*, 988−991.
(58) Chen, M.-H.; Hou, J.; Hong, Z.; Yang, G.; Sista, S.; Chen, L.-M.; Yang, Y. *Adv. Mater.* **2009**, *21*, 4238−4242.
(59) Marcus, R. A.; Sutin, N. *Biochim. Biophys. Acta* **1985**, *811*, 265−322.
(60) Tachiya, M. *J. Chem. Phys.* **1988**, *89*, 6929−6935.
(61) Braun, C. L. *J. Chem. Phys.* **1984**, *80*, 4157−4161.
(62) Hummelen, J. C.; Knight, B. W.; LePeq, F.; Wudl, F.; Yao, J.; Wilkins, C. L. *J. Org. Chem.* **1995**, *60*, 532−538.
(63) Jespersen, K. G.; Beenken, W. J. D.; Zaushitsyn, Y.; Yartsev, A.; Andersson, M.; Pullerits, T.; Sundström, V. *J. Chem. Phys.* **2004**, *121*, 12613−12617.
(64) As found for oligothiophenes (*n*T) with extrapolation to polythiophenes by means of correlated electron spin resonance and optical absorption spectroscopies (Horowitz, G.; Yassar, A.; von Bardeleben, H. J. *Synth. Met.* **1994**, *62*, 245−252), either the HOMO-to-LUMO band (P3) or the SOMO-to-LUMO + 1 band (P4) appears likely to the higher energy side of the SOMO-to-LUMO band (P2). However, whether the absorption peaking at 440 nm arises from $PFDTBT^{2+}$ deserves further studies.
(65) Jiang, X. M.; Österbacka, R.; Korovyanko, O.; An, C. P.; Horovitz, B.; Janssen, R. A. J.; Vardeny, Z. V. *Adv. Funct. Mater.* **2002**, *12*, 587−597.
(66) Österbacka, R.; An, C. P.; Jiang, X. M.; Vardeny, Z. V. *Science* **2000**, *287*, 839−842.
(67) Guo, J.; Ohkita, H.; Benten, H.; Ito, S. *J. Am. Chem. Soc.* **2009**, *131*, 16869−16880.
(68) Guo, J.; Ohkita, H.; Benten, H.; Ito, S. *J. Am. Chem. Soc.* **2010**, *132*, 6154−6164.
(69) Horowitz, G.; Yassar, A.; von Bardeleben, H. J. *Synth. Met.* **1994**, *62*, 245−252.
(70) Neves-Petersen, M. T.; Gryczynski, Z.; Lakowicz, J.; Fojan, P.; Pedersen, S.; Petersen, E.; Petersen, S. B. *Protein Sci.* **2002**, *11*, 588−600.
(71) Rose, A. *Concepts in Photoconductivity and Allied Problems*; Interscience: New York, 1963.
(72) Nelson, J. *Phys. Rev. B* **2003**, *67*, 155209.
(73) Guo, J.; Ohkita, H.; Yokoya, S.; Benten, H.; Ito, S. *J. Am. Chem. Soc.* **2010**, *132*, 9631−9637.
(74) The time origin (Δt = 0.00 ps) is defined as the time at the maximum of the cross-correlation trace between the pump and the probe pulses.
(75) Giaimo, J. M.; Gusev, A. V.; Wasielewski, M. R. *J. Am. Chem. Soc.* **2002**, *124*, 8530−8531.
(76) Lathrop, E. J. P.; Friesner, R. A. *J. Phys. Chem.* **1994**, *98*, 3056−3066.
(77) Laporte, L. L.; Palaniappan, V.; Davis, D. G.; Kirmaier, C.; Schenck, C. C.; Holten, D.; Bocian, D. F. *J. Phys. Chem.* **1996**, *100*, 17696−17707.
(78) Won, Y.; Friesner, R. A. *Proc. Natl. Acad. Sci. U.S.A.* **1987**, *84*, 5511−5515.
(79) Zhang, W.; Hu, R.; Li, D.; Huo, M.-M.; Ai, X.-C.; Zhang, J.-P. *J. Phys. Chem. C* **2012**, *116*, 4298−4310.
(80) Marsh, R. A.; Hodgkiss, J. M.; Friend, R. H. *Adv. Mater.* **2010**, *22*, 3672−3676.
(81) Mihailetchi, V. D.; Koster, L. J. A.; Hummelen, J. C.; Blom, P. W. M. *Phys. Rev. Lett.* **2004**, *93*, 216601.
(82) Coffey, D. C.; Larson, B. W.; Hains, A. W.; Whitaker, J. B.; Kopidakis, N.; Boltalina, O. V.; Strauss, S. H.; Rumbles, G. *J. Phys. Chem. C* **2012**, *116*, 8916−8923.
(83) Lee, J.; Vandewal, K.; Yost, S. R.; Bahlke, M. E.; Goris, L.; Baldo, M. A.; Manca, J. V.; Van Voorhis, T. *J. Am. Chem. Soc.* **2010**, *132*, 11878−11880.
(84) Etzold, F.; Howard, I. A.; Forler, N.; Cho, D. M.; Meister, M.; Mangold, H.; Shu, J.; Hansen, M. R.; Müllen, K.; Laquai, F. *J. Am. Chem. Soc.* **2012**, *134*, 10569−10583.
(85) Pensack, R. D.; Guo, C.; Vakhshouri, K.; Gomez, E. D.; Asbury, J. B. *J. Phys. Chem. C* **2012**, *116*, 4824−4831.
(86) Jamieson, F. C.; Domingo, E. B.; McCarthy-Ward, T.; Heeney, M.; Stingelin, N.; Durrant, J. R. *Chem. Sci.* **2012**, *3*, 485−492.
(87) Collins, B. A.; Gann, E.; Guignard, L.; He, X.; McNeill, C. R.; Ade, H. *J. Phys. Chem. Lett.* **2010**, *1*, 3160−3166.